A high-order finite volume remapping scheme for nonuniform grids: the piecewise quartic method (PQM)*

Laurent White†, Alistair Adcroft

March 26, 2008

Princeton University, Program in Atmospheric and Oceanic Sciences,
201 Forrestal Road, Princeton, NJ 08540, USA.

Abstract

A hierarchy of one-dimensional high-order remapping schemes is presented and their performance with respect to accuracy, convergence rate and dispersion investigated. The schemes are also compared based on traditional advection experiments in periodic domains and remapping experiments in closed domains. The piecewise quartic method (PQM) is presented, based on fifth-order accurate piecewise polynomials, and is motivated by the need to significantly improve hybrid coordinate systems of ocean climate models, which require the remapping to be conservative, monotonic and highly accurate. A limiter for this scheme is fully described that never decreases the polynomial degree, except at the location of extrema where a piecewise constant reconstruction is used. We assess the use of high-order explicit and implicit (i.e., compact) estimates for the edge values and slopes needed to build the piecewise polynomials in both PPM (piecewise parabolic method) and PQM. It is shown that all limited PQM schemes perform significantly better than limited PPM schemes and that PQM schemes are much more cost-effective.

Keywords: reconstruction; remapping; piecewise parabolic method (PPM); piecewise quartic method (PQM); finite volume method; nonuniform grids; compact schemes; advection schemes

1 Introduction

Remapping is a crucial component of most Arbitrary Lagrangian-Eulerian (ALE) algorithms used in computational fluid dynamics [12, 16, 13]. These algorithms involve a regridding step, whereby a new grid is generated based on some criteria, and a remapping step, whereby the variables are remapped from the old grid onto the new grid (Figure 1). It is generally required that remapping be both conservative and monotonic in the sense that no new extrema should be created nor existing ones amplified. This is particularly important in applications where boundedness of some variables must be guaranteed.

The present study is motivated by the growing need to improve vertical coordinate systems in ocean general circulation models used for climate predictions. Over the last four decades or so, the vast majority of ocean models have used a single coordinate system in the vertical, usually aiming at a better representation of selected physical processes. These ocean models, however,

*Revised manuscript submitted to the Journal of Computational Physics on ?? March 2008
†Corresponding author. E-mail: laurentw@princeton.edu, tel +1 609 452 5305, fax +1 609 987 5063.

have difficulties resolving physical processes for which they were not primarily designed. Hybrid coordinate ocean models have thus naturally emerged where the vertical grid is built by combining different coordinate systems in different regions [15, 2, 6, 1]. Due to the dynamical nature of the ocean, these hybrid coordinate systems are adapted in the course of the simulations, which means that vertical remapping is a key component. The accuracy of remapping is a major research issue in hybrid coordinate ocean models that prevents the hybrid framework from being truly convincing; presently, third-order reconstruction is used, at best, in these models. Hence, there is a need to explore higher-order representations.

An essential element of any remapping scheme lies in the reconstruction. Based on a set of cell averages on a given grid, the objective of a reconstruction scheme is to accurately and conservatively represent the underlying, real data with piecewise functions. Other constraints, such as monotonicity, may also apply. In this paper, we limit ourselves to piecewise polynomials but other functions can be employed, such as rational functions [e.g., 19]. Once the polynomial degree is chosen (for example, degree two leading to piecewise parabolas), a number of degrees of freedom must be determined that will produce a unique polynomial over the cell. There are basically two ways of improving a polynomial reconstruction method. First, the accuracy of the estimates for the pending degrees of freedom (e.g., edge values) may be improved. Second, when a monotonic reconstruction is required, improving the limiter may yield more accurate results. The latter domain of improvement, in particular, has drawn most of the attention in the case of the piecewise parabolic method (PPM) [4, 3, 11, 17, 10]. Besides these efforts, piecewise polynomial methods have witnessed almost no improvement regarding the edge estimates or the use of higher-degree polynomials. Only recently has the parabolic spline method been introduced but it also relies on polynomials of degree two [20]. [5] clearly showed that successively high-order schemes lead to more accurate solutions for both limited and unlimited finite volume fluxes. The close relationship between their third-order method and PPM inspired us to seek improvement by using higher-order polynomials.

The objective of this paper is twofold. First, we introduce the piecewise quartic method (PQM) that uses piecewise polynomials of degree four and which, to our knowledge, has never been presented before. A limiter is devised that ensures monotonicity of any PQM-based remapping scheme. Second, a range of explicit and implicit schemes to estimate the edge values and slopes is investigated on the basis of accuracy, convergence analysis and dispersion.

The main part (Section 2) of the paper focuses on reconstruction. We present PQM and the wide range of explicit and implicit schemes to estimate the edge values and slopes. The associated PPM and PQM schemes are evaluated in terms of accuracy. A limiter for PQM is also described in detail. Section 3 deals with remapping itself in the form of advection. Accuracy and dipersion analysis serve as comparative tools. The treatment of boundaries is covered in Section 4 and some comments on computational costs are made in Section 5. Conclusions are given in Section 6.

2 Piecewise polynomial reconstruction schemes

Given a nonuniform grid of cell widths h_j and cell averages $\bar{u}_j$, for $j = 1, 2 \dots N$ where N is the number of cells, the objective is to determine a piecewise polynomial reconstruction that accurately approximates the underlying data (Figure 2). The polynomial over cell j is noted R_j and, for convenience, use is made of a local coordinate $\xi \in [0, 1]$ such that the global coordinate x is given by

$$\begin{aligned} x &= x_{j-\frac{1}{2}} + \left(x_{j+\frac{1}{2}} - x_{j-\frac{1}{2}} \right) \xi \\ &= x_{j-\frac{1}{2}} + h_j \xi, \end{aligned} \tag{1}$$

where the global coordinates of the left and right cell interfaces are $x_{j-\frac{1}{2}}$ and $x_{j+\frac{1}{2}}$, respectively.

Whichever polynomial reconstruction is considered, we require the method to be locally conservative. Hence, the cell average of R_j must satisfy the following relationship :

$$\frac{1}{h_j}\int_{x_{j-\frac{1}{2}}}^{x_{j+\frac{1}{2}}} R_j(x)\,\mathrm{d}x = \int_0^1 R_j(\xi)\,\mathrm{d}\xi = \bar{u}_j, \tag{2}$$

which constrains one degree of freedom. A trivial choice is to resort to piecewise constants, in which case we simply have $R_j = \bar{u}_j$. The piecewise constant method (PCM) is only first-order accurate and, when combined with remapping, is highly diffusive and has poor dispersion properties. Improvement is gained by using a second-order accurate scheme based on a linear reconstruction. The piecewise linear method (PLM) requires an additional constraint. An estimate of the slope generally serves this purpose [18, 9]. Although more accurate and less diffusive than PCM, PLM performs poorly when extensive remapping occurs (e.g., many remapping steps or long integration times for advection problems). We now focus on third-order and fifth-order reconstruction methods, referred to as the piecewise parabolic method (PPM) and the piecewise quartic method (PQM), respectively.

2.1 The piecewise parabolic method (PPM)

With the piecewise parabolic method, a parabola is constructed within each cell. The general form is

$$P(\xi) = a_0 + a_1\xi + a_2\xi^2 \tag{3}$$

and three coefficients need be determined. In addition to the enforcement of local conservation, Eq. (2), two additional constraints are necessary. A natural choice is to enforce the value of the parabola at the left and right edges of the cell. If these edge values are noted u_L and u_R, respectively, and if the cell average is denoted by $\bar{u}$, the coefficients of the parabola are

$$\begin{aligned} a_0 &= u_L, \\ a_1 &= 6\bar{u} - 4u_L - 2u_R, \\ a_2 &= 3\left(u_L + u_R - 2\bar{u}\right). \end{aligned} \tag{4}$$

The remaining part of the reconstruction process is to estimate the edge values. This is also where much liberty is afforded. We note that low-order estimates of the edge values will impair the overall quality of the reconstruction scheme. In particular, estimates of edge values should be at least third-order accurate in order for a global parabolic profile to be exactly retrieved by a reconstruction scheme based on PPM. Any higher-order estimates of edge values will provide a piecewise parabolic reconstruction that also passes this sanity check.

2.2 The piecewise quartic method (PQM)

The piecewise quartic method relies on piecewise polynomials of degree four:

$$Q(\xi) = a_0 + a_1\xi + a_2\xi^2 + a_3\xi^3 + a_4\xi^4. \tag{5}$$

Five coefficients have to be determined and, therefore, four constraints are needed in addition to local conservation, Eq. (2). Similarly to PPM, the edge values provide two constraints. Two natural additional constraints are the edge slopes. Given the left and right edge slopes u'_L and u'_R,

respectively, and keeping the same notations for the edge values and cell average as before, the five coefficients read

$$\begin{aligned} a_0 &= u_L, \\ a_1 &= u'_L, \\ a_2 &= 30\bar{u} - 12u_R - 18u_L + \frac{3}{2}\left(u'_R - 3u'_L\right), \\ a_3 &= -60\bar{u} + 6u'_L - 4u'_R + 28u_R + 32u_L, \\ a_4 &= 30\bar{u} + \frac{5}{2}\left(u'_R - u'_L\right) - 15\left(u_L + u_R\right), \end{aligned} \tag{6}$$

where

$$\begin{aligned} u'_L &= \frac{\partial Q}{\partial \xi}|_{\xi=0} = \frac{\partial Q}{\partial x}|_{x=x_{j-\frac{1}{2}}} h_j, \\ u'_R &= \frac{\partial Q}{\partial \xi}|_{\xi=1} = \frac{\partial Q}{\partial x}|_{x=x_{j+\frac{1}{2}}} h_j. \end{aligned}$$

The above relationships are easily derived from Eq. (1).

Again, care must be taken to use estimates that are sufficiently accurate in order to exactly retrieve a global quartic profile. Hence, at least fifth-order accurate edge values and at least fourth-order accurate edge slopes should be used to be consistent with the order of the polynomials used for the reconstruction. Because both the edge values and slopes must be provided, a great number of possible combinations is theoretically possible.

We now turn our attention to the estimation of edge values and slopes by using both explicit and implicit (i.e., compact) schemes.

2.3 Edge-value estimates

To estimate the edge values, explicit or implicit schemes can be used. We refer to explicit schemes as those schemes that provide estimates via closed-form expressions. Implicit schemes, on the other hand, require solving a linear system. Explicit schemes have the advantage of being computationally cheaper than implicit schemes because, unlike implicit schemes, they do not require solving banded diagonal systems. However, for a given order of accuracy, implicit schemes are globally more accurate and the stencil is shorter than for explicit schemes. This is a clear advantage when boundaries are involved. In addition, as will be shown, remapping schemes based on implicit estimates of edge values are less diffusive and have better dispersion properties. For the sake of clarity, the following discussion deals with uniform grids. The equivalent expressions for nonuniform grids are provided in the Appendix.

2.3.1 Explicit schemes

All explicit schemes are based on fitting (in a finite volume sense) a polynomial through the data and evaluating it at the location of an edge to obtain an estimate of the edge value. When evaluated pointwise, a fitting polynomial of degree $n-1$, based on data in n cells, provides an n^{th}-order accurate estimate of the edge value. It is assumed that the degrees of cell-centered and edge-centered polynomials are even and odd, respectively (Figure 3). Edge-centered polynomials are unique to each edge and therefore provide a unique estimate for the edge value. Cell-centered polynomials are unique to each cell and provide the left and right edge values for this cell. In this case, neighboring estimates may be different so that two different edge value estimates may be associated with a given edge, giving rise to a piecewise discontinuous reconstruction.

Fitting in a finite volume sense means that a polynomial F_k of even degree n and centered on cell k satisfies the following relationships

$$\frac{1}{h_j}\int_{x_{j-\frac{1}{2}}}^{x_{j+\frac{1}{2}}} F_k(x)\,\mathrm{d}x = \bar{u}_j \qquad \text{for} \quad j = k-\frac{n}{2},\dots j+\frac{n}{2}, \tag{7}$$

while a polynomial $F_{k+\frac{1}{2}}$ of odd degree n and centered on edge $k+\frac{1}{2}$ satisfies the following relationships

$$\frac{1}{h_j}\int_{x_{j-\frac{1}{2}}}^{x_{j+\frac{1}{2}}} F_{k+\frac{1}{2}}(x)\,\mathrm{d}x = \bar{u}_j \qquad \text{for} \quad j = k-\underline{\frac{n}{2}},\dots j+\overline{\frac{n}{2}}, \tag{8}$$

where the underline and overline indicate rounding down and up, respectively, to the closest integer.

As inspired by [7], edge-value estimates are provided for cell j, in which case we have $u_L = u_{j-\frac{1}{2}}$ and $u_R = u_{j+\frac{1}{2}}$.

Third-order estimates on uniform grids are given by

$$\begin{aligned} u_{j-\frac{1}{2}} &= \frac{1}{6}\left(2\bar{u}_{j-1}+5\bar{u}_j-\bar{u}_{j+1}\right), \\ u_{j+\frac{1}{2}} &= \frac{1}{6}\left(-\bar{u}_{j-1}+5\bar{u}_j+2\bar{u}_{j+1}\right), \end{aligned} \tag{9}$$

and will be referred to as h_3 estimates.

Fourth-order estimates on uniform grids are given by

$$\begin{aligned} u_{j-\frac{1}{2}} &= \frac{1}{12}\left(-\bar{u}_{j-2}+7\bar{u}_{j-1}+7\bar{u}_j-\bar{u}_{j+1}\right), \\ u_{j+\frac{1}{2}} &= \frac{1}{12}\left(-\bar{u}_{j-1}+7\bar{u}_j+7\bar{u}_{j+1}-\bar{u}_{j+2}\right), \end{aligned} \tag{10}$$

and will be referred to as h_4 estimates.

Fifth-order estimates on uniform grids are given by

$$\begin{aligned} u_{j-\frac{1}{2}} &= \frac{1}{60}\left(-3\bar{u}_{j-2}+27\bar{u}_{j-1}+47\bar{u}_j-13\bar{u}_{j+1}+2\bar{u}_{j+2}\right), \\ u_{j+\frac{1}{2}} &= \frac{1}{60}\left(2\bar{u}_{j-2}-13\bar{u}_{j-1}+47\bar{u}_j+27\bar{u}_{j+1}-3\bar{u}_{j+2}\right), \end{aligned} \tag{11}$$

and will be referred to as h_5 estimates.

Sixth-order estimates on uniform grids are given by

$$\begin{aligned} u_{j-\frac{1}{2}} &= \frac{1}{60}\left(\bar{u}_{j-3}-8\bar{u}_{j-2}+37\bar{u}_{j-1}+37\bar{u}_j-8\bar{u}_{j+1}+\bar{u}_{j+2}\right), \\ u_{j+\frac{1}{2}} &= \frac{1}{60}\left(\bar{u}_{j-2}-8\bar{u}_{j-1}+37\bar{u}_j+37\bar{u}_{j+1}-8\bar{u}_{j+2}+\bar{u}_{j+3}\right), \end{aligned} \tag{12}$$

and will be referred to as h_6 estimates.

Note that averaging the discontinuous h_3 and h_5 estimates lead to the h_4 and h_6 estimates, respectively.

2.3.2 Implicit schemes

Limiting ourselves to tridiagonal systems for computational efficiency, a general expression for implicit (or compact) schemes on nonuniform grids, relating edge values to cell averages, is given by

$$\alpha u_{j-\frac{1}{2}} + u_{j+\frac{1}{2}} + \beta u_{j+\frac{3}{2}} = a\bar{u}_{j-1} + b\bar{u}_j + c\bar{u}_{j+1} + d\bar{u}_{j+2}, \tag{13}$$

[8]. Note that, in Eq. (13), pointwise values appear in the left-hand side while cell averages appear in the right-hand side. The unknown coefficients α, β and a, b, c, d are determined via a Taylor expansion of u about $j+\frac{1}{2}$, as presented by [8]. The desired order of accuracy is attained by having terms of lower matching orders of accuracy cancel out, which yields equations to be satisfied by the unknown coefficients. In the particular case of uniform grids, Eq. (13) is symmetric about $u_{j+\frac{1}{2}}$ so that $\alpha = \beta$, $a = d$ and $b = c$.

In principle, odd-order accurate edge-value estimates could be calculated but it would imply considering asymmetric stencils. For example, a third-order estimate can be obtained by computing α, β and a while $b = c = d = 0$. The unknowns would then be determined by enforcing the zeroth-, first- and second-order terms to cancel out in the Taylor expansion. However, asymmetric estimates for the edge values should not be used since they produce asymmetric reconstructions even for symmetric data.

The coefficients α, β and a, b, c, d are given in Table 1 for uniform grids. Implicit edge-value estimates will be referred to as ih_n, where n is the order of accuracy.

2.4 Edge-slope estimates

Similarly to edge values, estimates for edge slopes may be based on explicit or implicit schemes. Uniform grids are assumed for the sake of clarity in the following discussion.

2.4.1 Explicit schemes

Explicit edge-slope estimates of $n^{th}-$order accuracy are calculated by first determining the fitting polynomial of degree n. The polynomial is then differentiated and the resulting polynomial (of degree $n-1$) is evaluated pointwise to yield a slope estimate. The estimates are continuous, even when using cell-centered fitting polynomials.

Fourth-order estimates on uniform grids are given by

$$\begin{aligned} u'_{j-\frac{1}{2}} &= \frac{1}{12h}\left[15\left(\bar{u}_j - \bar{u}_{j-1}\right) - \left(\bar{u}_{j+1} - \bar{u}_{j-2}\right)\right], \\ u'_{j+\frac{1}{2}} &= \frac{1}{12h}\left[15\left(\bar{u}_{j+1} - \bar{u}_j\right) - \left(\bar{u}_{j+2} - \bar{u}_{j-1}\right)\right], \end{aligned} \tag{14}$$

and will be referred to as h_4 estimates.

Fifth-order estimates on uniform grids are given by

$$\begin{aligned} u'_{j-\frac{1}{2}} &= \frac{1}{180h}\left[245\left(\bar{u}_j - \bar{u}_{j-1}\right) - 25\left(\bar{u}_{j+1} - \bar{u}_{j-2}\right) + 2\left(\bar{u}_{j+2} - \bar{u}_{j-3}\right)\right], \\ u'_{j+\frac{1}{2}} &= \frac{1}{180h}\left[245\left(\bar{u}_{j+1} - \bar{u}_j\right) - 25\left(\bar{u}_{j+2} - \bar{u}_{j-1}\right) + 2\left(\bar{u}_{j+3} - \bar{u}_{j-2}\right)\right], \end{aligned} \tag{15}$$

and will be referred to as h_5 estimates.

2.4.2 Implicit schemes

Again, limiting ourselves to tridiagonal systems for computational efficiency, a general expression for implicit (or compact) schemes on nonuniform grids, relating edge slopes to cell averages, is given by

$$\alpha u'_{j-\frac{1}{2}} + u'_{j+\frac{1}{2}} + \beta u'_{j+\frac{3}{2}} = a\bar{u}_{j-1} + b\bar{u}_j + c\bar{u}_{j+1} + d\bar{u}_{j+2}. \tag{16}$$

The unknown coefficients α, β and a, b, c, d are determined via a Taylor expansion of u about $j+\frac{1}{2}$. The desired order of accuracy is attained by having terms of lower matching orders of accuracy cancel out, which yields equations to be satisfied by the unknown coefficients. In the particular case of uniform grids, Eq. (16) is symmetric about $u_{j+\frac{1}{2}}$ so that $\alpha = \beta$, $a = -d$ and $b = -c$. Note also that, because of this symmetry, implicit schemes on uniform grids produce edge-slope estimates that are automatically one order of accuracy higher than their equivalent on nonuniform grids. Hence, for example, by designing a third-order scheme for nonuniform grids, it becomes automatically fourth-order accurate on uniform grids. This gain in accuracy does not happen when estimating edge values.

The coefficients α, β and a, b, c, d are given in Table 2 for uniform grids. Implicit edge-slope estimates will be referred to as ih_n, where n is the *actual* order of accuracy. So, n may change depending on whether uniform or nonuniform grids are actually used, although the same scheme is considered.

2.5 Reconstruction accuracy and convergence analysis

We now compare PPM and PQM solely on the basis of unlimited reconstruction performance. Remapping errors will be analyzed later. We aim at assessing how edge-value and edge-slope estimates affect the global error of the scheme and its order of accuracy. The global error is a measure (for a given norm) of the error on a given grid while the order of accuracy is the rate at which this global error decreases as the grid size decreases. Both measures must be considered. Indeed, schemes using h_n and ih_n estimates for the edge values will have the same order of accuracy but will most likely have different error norms on a given grid.

A PPM scheme denoted by PPM h_n means that h_n edge-value estimates are used for reconstruction. Similarly, a PQM scheme denoted by PQM h_n/h_m means that h_n edge-value and h_m edge-slope estimates are used for the reconstruction. Generally, for consistency, we require that the order of accuracy for the edge-value estimates be one unit higher than that for the edge-slope estimates (i.e., $n = m + 1$).

To avoid having to deal with boundaries, periodic domains will first be considered. The treatment of boundaries is covered in Section 4. A periodic function $f(x)$ is given as initial data on the nondimensional domain $[0, 1]$. Initial cell averages are defined as follows:

$$\bar{u}_j = \frac{1}{h_j} \int_{x_{j-\frac{1}{2}}}^{x_{j+\frac{1}{2}}} f(x)\, \mathrm{d}x.$$

Reconstruction accuracy is evaluated by calculating the L_2-norm of the error e:

$$||e||_{L_2} = \left[\int_0^1 |f(x) - R(x)|^2 \, \mathrm{d}x \right]^{1/2},$$

where R is the global reconstructed profile, made up of piecewise polynomials R_j defined on each cell. The polynomials R_j are defined by (3)-(4) and (5)-(6) for PPM and PQM, respectively. Examples of reconstructions using PPM and PQM are shown in Figure 4. For both methods, implicit

edge-value estimates produce more accurate results than their explicit equivalent for a given order of accuracy. In addition, at low resolution, PPM ih_4 yields a reconstruction that is more accurate than both high-order explicit PQM h_5/h_4 and PQM h_6/h_5 schemes. Therefore, to be a successful alternative to PPM with implicit edge-value estimates at lower resolutions, PQM must also make use of implicit edge-value estimates.

Now, since the orders of accuracy of PPM and PQM are three and five, respectively, we expect all PQM schemes to to be more accurate than PPM schemes at higher resolutions. This is shown via a convergence analysis experiment where gradually refined uniform and nonuniform grids are used for reconstructing the Gaussian profile on a periodic domain (Figure 5). Nonuniform grids are simply modified uniform grids for which the edge locations are perturbed by a uniformly-distributed number in $[-h/4, h/4]$, where h is the uniform grid size. For uniform grids, the error norms are reported against h while for nonuniform random grids, error norms are reported against the average grid size $\bar{h}$.

As shown in Figure 5, using at least third-order accurate edge-value estimates for PPM ensures that the scheme is third-order accurate. Similarly, using edge-value and edge-slope estimates that are at least fifth-order and fourth-order accurate, respectively, ensures that PQM is fifth-order accurate. Note, however, that the empirical reconstruction order of accuracy for PQM h_6/h_5 and PQM ih_6/ih_5 is six. Finally, as expected, the order of accuracy of PQM ih_4/ih_3 reduces to four.

In agreement with results shown in Figure 4, not only do implicit schemes perform better than their explicit equivalent overall, they especially produce more accurate reconstructions at lower resolutions (see inset in Figure 5a), which are resolutions that usually matter in most applications. At low resolution, PPM ih_4 is more accurate than all explicit PQM schemes but PQM ih_4/ih_3 and PQM ih_6/ih_5 perform better. Nonetheless, as already mentioned, PQM ih_4/ih_3 is fourth-order accurate, which turns out to be a waste of the potentially higher order of accuracy of PQM .

2.6 Limiting PQM

We now take up the task of limiting the PQM reconstruction scheme in order to obtain piecewise quartics that are monotonic within each cell and bounded between neighboring cell averages. This ensures that the PQM-based remapping scheme will neither create new extrema nor amplify existing ones.

The algorithm for limiting PQM operates in two phases. The first phase ensures that the edge values are bounded by neighboring cell averages and that the edge slopes are consistent by being of the same sign as that of the limited PLM slope. Once the edge values and slopes are bounded and consistent, respectively, the second phase ensures that the ensuing quartic is monotonic within the cell. This requires checking whether inflexion points exist within the cell and, if so, whether the slope of the quartic at the inflexion points is of the same sign as that of the limited PLM slope.

Before delving into the detailed algorithm, preliminary results regarding inflexion points are recalled.

Lemma 1 Any quartic $Q(\xi)$, as defined by (5)-(6) for $\xi \in [0, 1]$, has at most two inflexion points in $[0, 1]$.

Proof. Inflexion points are real roots of the second derivative of $Q(\xi)$, which is a parabola that has at most two real roots. QED.

Lemma 2 If the edge slopes are positive (negative) and if the derivative of the quartic $Q(\xi)$ at any inflexion point lying within $[0,1]$ is positive (negative), $Q(\xi)$ monotonically increases (decreases) in $[0,1]$.

Proof (for the positive case). Any inflexion point is an extremum of the derivative of $Q(\xi)$. If all extrema of the derivative in $[0,1]$ are positive, the derivative of $Q(\xi)$ is everywhere positive in $[0,1]$ and $Q(\xi)$ monotonically increases in $[0,1]$. QED.

Corollary 1 If the edge slopes are positive ($u'_L > 0$ and $u'_R > 0$) and if the quartic $Q(\xi)$ has no inflexion point lying within $(0,1)$, $Q(\xi)$ monotonically increases in $[0,1]$.

Proof. This follows from Lemma 2. Note that inflexion points lying on either edge (and only there) do not preclude the quartic to be monotonic.

Since the limited PLM slope is resorted to throughout the algorithm, we now give its definition for nonuniform grids. Given a cell of width h_C and left and right neighboring cells of widths h_L and h_R, respectively, the limited PLM slope σ is defined as

$$\sigma = \begin{cases} \text{sign}(\sigma_C)\min\left(|\sigma_L|, |\sigma_R|, |\sigma_C|\right) & \text{if } \sigma_L\sigma_R > 0, \\ 0 & \text{otherwise}, \end{cases} \tag{17}$$

where σ_L and σ_R are the left and right one-sided slopes, respectively, and σ_C is the centered slope. The sign function is equal to 1 for positive arguments, -1 for negative arguments and 0 otherwise. The one-sided and centered slopes are defined as

$$\begin{aligned} \sigma_L &= 2\frac{\bar{u}_C - \bar{u}_L}{h_L + h_C} \times \frac{h_L + h_C}{h_C} = 2\frac{\bar{u}_C - \bar{u}_L}{h_C}, \\ \sigma_R &= 2\frac{\bar{u}_R - \bar{u}_C}{h_C + h_R} \times \frac{h_C + h_R}{h_C} = 2\frac{\bar{u}_R - \bar{u}_C}{h_C}, \\ \sigma_C &= 2\frac{\bar{u}_R - \bar{u}_L}{h_L + 2h_C + h_R}, \end{aligned} \tag{18}$$

where $\bar{u}_L$, $\bar{u}_C$ and $\bar{u}_R$ are the cell averages associated with the left, center and right cells, respectively. Note that the slopes defined by Eq. (18) are the traditional van Leer limited PLM slopes [e.g., 9], written for nonuniform grids. An illustration is provided in Figure 6.

Both phases of the algorithm are now described in detail. We assume that edge values u_L and u_R and edge slopes u'_L and u'_R are given.

2.6.1 Edge values boundedness and edge slopes consistency

Prior to any verification of boundedness and consistency, local extrema are flattened by equating the edge values to the cell average and the edge slopes to zero. An extremum is detected when the left and right one-sided slopes have different signs, which, according to Eq. (17), translates into $\sigma = 0$. If no extremum is detected, the boundedness of edge values is checked.

An edge value is limited only when it is unbounded, that is, when it lies out of the range defined by the neighboring cell averages. If the calculated edge value is bounded, we assume that the estimate is accurate and need not be modified. Hence, if the left edge value is unbounded, that is if

$$(\bar{u}_L - u_L)(u_L - \bar{u}_C) < 0,$$

then the new estimate reads:

$$u_L \leftarrow \bar{u}_C - \text{sign}\,(\sigma) \min\left(\frac{h_C}{2}|\sigma|, |u_L - \bar{u}_C|\right). \tag{19}$$

Similarly, if the right edge value is unbounded, that is if

$$(\bar{u}_R - u_R)(u_R - \bar{u}_C) < 0,$$

then the new estimate reads:

$$u_R \leftarrow \bar{u}_C + \text{sign}\,(\sigma) \min\left(\frac{h_C}{2}|\sigma|, |u_R - \bar{u}_C|\right). \tag{20}$$

An illustration of how these limiters operate is provided in Figure 7. A final check is conducted to make sure that discontinuous edge values are monotonic at any edge. If edge values are discontinuous and nonmonotonic, they are both replaced by their average.

Finally, consistency checks are performed on edges slopes. For consistency, the edge slopes must be of the same sign as that of the limited PLM slope σ. Each slope having the wrong sign is set to be equal to σ. Among other choices, such as setting the slope to zero or to the one-sided slope, this was empirically found to produce more accurate results.

Three cases need be considered: (1) The slopes are of the same sign, which is the sign of σ. No modification is carried out; (2) The slopes are of the same sign, which is opposite to that of σ. Both slopes are equated to σ; (3) The left and right edge slopes may be of different sign. This usually happens for edge slopes located on either side of an extremum, which is then taken care of at the beginning of the algorithm through extremum detection. It may also happen, however, for monotonic data. In that case, the slope having the wrong sign is equated to σ.

2.6.2 Monotonicity enforcement

At this point of the algorithm, extrema are flattened, edge values are bounded and edge slopes are consistent with the limited PLM slope σ. Yet, this does not guarantee piecewise monotonicity (see examples thereof in Figure 8), which is now addressed.

Monotonicity is guaranteed whenever $Q(\xi)$ has no inflexion point (see Corollary 1). When $Q(\xi)$ has any inflexion point, monotonicity is guaranteed provided that the derivative of $Q(\xi)$ at the location of inflexion points be of the same sign as that of the limited PLM slope (Lemma 2). That is, the inflexion points must be consistent with the PLM slope (see, e.g., Figure 8d that features a quartic with two consistent inflexion points). Considering the locations of inflexion points rather than the locations of extrema is simpler because it involves parabolas rather than cubics, the former being much more amenable to analytical manipulations.

The algorithm that enforces monotonicity functions as follows. We first check for the existence of inflexion points by computing the roots of the second derivative of $Q(\xi)$, $Q^{(2)}(\xi)$. If none lies in $[0, 1]$, the quartic is monotonic. If there is at least one inflexion point, the associated slope is

calculated at the location of each one of these inflexion points and compared with the limited PLM slope. If the slopes are consistent, $Q(\xi)$ is monotonic. If the slopes are not consistent, we enforce $Q(\xi)$ to have two inflexion points collapse – i.e., $Q^{(2)}(\xi)$ has one double root – on either edge, the choice of which depends on the relative values of the one-sided PLM slopes. The decision is made as follows:

$$\begin{array}{rcl} |\sigma_L| \leq |\sigma_R| & \Rightarrow & \text{collapse inflexion points on left edge,} \\ |\sigma_R| < |\sigma_L| & \Rightarrow & \text{collapse inflexion points on right edge,} \end{array} \tag{21}$$

where the slopes are defined by Eq. (18).

Mathematical convenience is one of the motives behind the choice of having inflexion points collapse onto either one of the edges. The other reason is that a quartic having this property, as dictated by (21), has a single-signed curvature. The sign of the curvature automatically produces a quartic that is shaped like the underlying three-cell data set (the left, center and right cell averages). This is so because the sign of the curvature is simultaneously controlled by (a) whether the underlying three-cell data set increases or decreases and (b) where inflexion points are located, which, according to (21), is also where the smallest one-sided PLM slope is located. For example, let us assume that the data set increases and that the smallest one-sided slope is the left one. Then, the only possibility is a positive curvature, which means that the derivative increases from its minimum on the left (where both inflexion points are located). This, in turn, means that the reconstructed quartic has a steeper slope on the right, which is consistent with the fact that the right one-sided slope is larger too (this particular case is illustrated in Figure 9).

The second derivative of the quartic, $Q^{(2)}(\xi)$, can be written as

$$Q^{(2)}(\xi) = b_0 + b_1\xi + b_2\xi^2, \tag{22}$$

where the coefficients b_0, b_1 and b_2 are related to the original coefficients of the quartic $Q(\xi)$ – see Eqs (5) and (6) – as follows:

$$\begin{array}{rcccl} b_0 & = & 2a_2 & = & 60\bar{u} - 24u_R - 36u_L + 3\left(u'_R - 3u'_L\right), \\ b_1 & = & 6a_3 & = & -360\bar{u} + 36u'_L - 24u'_R + 168u_R + 192u_L, \\ b_2 & = & 12a_4 & = & 360\bar{u} + 30\left(u'_R - u'_L\right) - 180\left(u_L + u_R\right). \end{array} \tag{23}$$

Let ξ_1 and ξ_2 denote the roots of $Q^{(2)}(\xi)$. Those roots satisfy the following relationships:

$$\begin{array}{rcl} \xi_1 + \xi_2 & = & -\dfrac{b_1}{b_2}, \\ \xi_1\xi_2 & = & \dfrac{b_0}{b_2}. \end{array}$$

When both roots are located on the left edge, at $\xi = 0$, we have

$$\begin{array}{rcccl} \xi_1 + \xi_2 & = & 0 & \Rightarrow & b_1 = 0, \\ \xi_1\xi_2 & = & 0 & \Rightarrow & b_0 = 0. \end{array} \tag{24}$$

When the roots are located on the right edge, at $\xi = 1$, we have

$$\begin{array}{rcccl} \xi_1 + \xi_2 & = & 2 & \Rightarrow & b_1 = -2b_2, \\ \xi_1\xi_2 & = & 1 & \Rightarrow & b_0 = b_2. \end{array} \tag{25}$$

Once a decision is made as to where both inflexion points should be located, Eqs (24) and (25), together with Eq. (23), give us relationships that must be satisfied by the four modifiable parameters: the edge values and edge slopes. Because the edge values have a higher impact on the global accuracy of the scheme, we prefer to first modify the edge slopes and leave the edge values intact.

Inflexion points on the left Let us first treat the case of both inflexion points on the left. Using Eqs (23) and (24), the edge slopes must be adjusted to

$$u'_L = \frac{1}{3}\left(10\bar{u} - 2u_R - 8u_L\right), \tag{26}$$

$$u'_R = -10\bar{u} + 6u_R + 4u_L. \tag{27}$$

It may happen, however, that the above solution provides an edge slope that is inconsistent with the limited PLM slope σ. When this happens, the quartic curvature is still single-signed but it is not monotonic because the derivative of $Q(\xi)$ reaches zero somewhere. This means that, given the edge values, there are no consistent edge slopes that produce a monotonic quartic. Note that, because the quartic curvature is single-signed, at most one edge slope could be inconsistent. When this situation turns up, one of the edge values must be modified. The inconsistent edge slope is first made equal to zero while the opposite edge slope and edge value are adjusted to build a new quartic that still possesses both inflexion points on the left. So, if the left edge slope is inconsistent, it is set to zero and the right edge value and slope are adjusted. If the right edge slope is inconsistent, it is set to zero while the left edge value and slope are adjusted. Mathematically, if $u'_L\sigma < 0$ then

$$\begin{aligned} u'_L &= 0, \\ u_R &= 5\bar{u} - 4u_L, \\ u'_R &= 20\left(\bar{u} - u_L\right), \end{aligned} \tag{28}$$

and if $u'_R\sigma < 0$ then

$$\begin{aligned} u'_R &= 0, \\ u_L &= \frac{1}{2}\left(5\bar{u} - 3u_R\right), \\ u'_L &= \frac{10}{3}\left(-\bar{u} + u_R\right). \end{aligned} \tag{29}$$

The adjustments (28) and (29), if carried out, are definitive in that the associated quartic is guaranteed to be monotonic and bounded by neighboring cell averages. Monotonicity directly follows from the fact that both edge slopes are consistent and that the curvature is single-signed. Boundedness is ensured by the property that the adjusted edge values are themselves bounded by their previous values and the cell average. This can be shown as follows. Without loss of generality, we assume that the underlying data set is increasing. We further assume that both edge values are bounded and that the edge slopes have been adjusted according to (26)-(27) to produce a quartic with inflexion points on the left. Now, we make the final assumption that the left edge slope is negative and, therefore, inconsistent (because the set of cell averages is increasing). Using (26), the right edge value is equal to

$$u_R = 5\bar{u} - 4u_L - \frac{3}{2}u'_L > 5\bar{u} - 4u_L, \tag{30}$$

the last inequality holding true because the left edge slope is negative. Because the left edge slope is inconsistent and set to zero, the right edge value is adjusted to $5\bar{u} - 4u_L$, following (28). As expressed by the inequality (30), this new edge value is smaller than the previous value, before adjustment. Since $u_L < \bar{u}$, it also remains bounded below by the cell average. Hence, the adjusted right edge value remains bounded by neighboring cell averages. The same reasoning applies for the case where the right edge slope is inconsistent and the left edge value must be adjusted (see Figure 10 for illustrations of both cases).

Inflexion points on the right The case where both inflexion points collapse onto the right edge is treated in a similar fashion. Using Eqs (23) and (25) , we find that the edge slopes must be adjusted to

$$u'_L = 10\bar{u} - 4u_R - 6u_L, \tag{31}$$

$$u'_R = \frac{1}{3}\left(-10\bar{u} + 8u_R + 2u_L\right). \tag{32}$$

Again, one of these slopes could be inconsistent with respect to the limited PLM slope σ. When this occurs, the inconsistent edge slope is set to zero while the opposite edge slope and edge value are adjusted to produce a quartic that still has both inflexion points on the right. If $u'_L\sigma < 0$ then

$$\begin{aligned} u'_L &= 0, \\ u_R &= \frac{1}{2}\left(5\bar{u} - 3u_L\right), \\ u'_R &= \frac{10}{3}\left(\bar{u} - u_L\right), \end{aligned} \tag{33}$$

and if $u'_R\sigma < 0$ then

$$\begin{aligned} u'_R &= 0, \\ u_L &= 5\bar{u} - 4u_R, \\ u'_L &= 20\left(-\bar{u} + u_R\right). \end{aligned} \tag{34}$$

In both cases, (33) and (34) provide adjusted edge values that are bounded by the cell average and the previous value, before adjustment. Hence, the quartic obtained is both monotonic and bounded.

2.6.3 Overall algorithm

The overall algorithm is now summarized.

1. Check whether the current cell average is an extremum. If so, flatten the quartic (a piecewise constant is used).
2. Check whether the edge values are bounded by the neighboring cell averages. If not, use (19) and (20) to bound the left and right edge values, respectively.
3. Check whether the edge slopes are consistent, that is, of the same sign as that of the limited PLM slope σ. If not, substitute σ for any inconsistent edge slope.
4. Check for the existence of inflexion points in $[0, 1]$. The quartic is bounded and monotonic (i.e., definitive) in the following cases: (a) no inflexion point, (b) one consistent inflexion point and (c) two consistent inflexion points. On the other hand, if one inflexion point is inconsistent (see e.g., Figure 8a-c), we enforce monotonicity by having both inflexion points collapse on either one of the edges, the choice of which depends on the following criteria:
   (i) if the left one-sided PLM slope has a smaller absolute magnitude than that of the right one ($\sigma_L <= \sigma_R$), both inflexion points are shifted to the left edge. This is done by modifying the edge slopes via Eqs (26)-(27) and, if required, by readjusting one if the edge values via Eq. (28) or Eq. (29).
   (ii) otherwise, both inflexion points are shifted to the right edge. Edge slopes are modified using Eqs (31)-(32) and, if necessary, one of the edge values is readjusted by using Eq. (33) or Eq. (34).

The first phase of the algorithm comprises steps (1)-(3) and provides bounded edge values and consistent edge slopes. The second phase of the algorithm, step (4), modifies the edge slopes and, if necessary, the edge values in order to obtain a monotonic quartic within each cell. In addition to edge-value boundedness and edge-slope consistency, this monotonicity constraint is a sufficient condition for having a remapping scheme that neither creates new extrema nor amplify existing ones. Yet, this condition is not necessary since a nonmonotonic quartic that is nevertheless everywhere bounded by neighboring cell averages will also yield a remapping scheme having these properties. Nonetheless, quartics that are nonmonotonic may lead to artificial steepening, a property that is usually beneficial to resolve extrema but may unrealistically steepen smooth profiles. Illustrations of the second phase of the algorithm are shown in Figure 10. The first phase is more straightforward and was partly presented in Figure 7.

3 Advection as a particular case of remapping

Let us assume that the following one-dimensional advection equation is to be solved on the periodic domain $[0, 1]$:

$$\frac{\partial u}{\partial t} + \frac{\partial u}{\partial x} = 0, \tag{35}$$

where the scalar u is the advected quantity and the advective velocity is unity. On a fixed grid, finite-volume advection schemes typically rely on fluxes across cell interfaces. Those fluxes are computed based on cellwise reconstructions. For CFL numbers greater than one, the computation of fluxes becomes less straightforward since they not only involve adjacent cells but also cells located further away. Therefore, a more natural way of thinking of advection is as a remapping scheme. At a given time step, the global profile is reconstructed by means of piecewise polynomials, shifted forwards (for positive advection speed) over a distance covered in one time step and overlaid on the grid to compute the new cell averages. Equivalently, the grid can be thought of being shifted backwards. This easily provides a way to advect quantities on nonuniform grids for CFL numbers greater than unity.

In this section, a dispersion analysis of unlimited remapping schemes is presented for the solution to Eq. (35) on uniform grids and CFL numbers smaller than unity. We then compare the limited schemes in their ability to accurately solve Eq. (35) on uniform and nonuniform grids for various initial conditions on periodic domains.

3.1 Dispersion analysis

Let us assume the grid to be uniform of cell size h. The time step is denoted by Δt and the CFL number is denoted by $\mu = \Delta t/h$. A flux-form, explicit, discrete version of Eq. (35) is

$$\bar{u}_j^{n+1} = \bar{u}_j^n + q_{j-\frac{1}{2}}^n - q_{j+\frac{1}{2}}^n, \tag{36}$$

where $q_{j-\frac{1}{2}}^n$ and $q_{j+\frac{1}{2}}^n$ are the fluxes across edges $j - \frac{1}{2}$ and $j + \frac{1}{2}$, respectively, that is the incoming and outgoing fluxes, respectively. The fluxes are computed as follows

$$\begin{aligned} q_{j-\frac{1}{2}}^n &= \int_{1-\mu}^{1} R_{j-1}(\xi)\, \mathrm{d}\xi, \\ q_{j+\frac{1}{2}}^n &= \int_{1-\mu}^{1} R_{j}(\xi)\, \mathrm{d}\xi, \end{aligned}$$

where R_j is the local polynomial reconstruction in cell j. The local polynomial R_j depends on the edge-value estimates (and also the edge-slope estimates in case of PQM), which, in turn, depend on cell averages. Hence, the fluxes can be expressed explicitly in terms of cell averages by using formulae presented in Sections 2.3 and 2.4.

Assuming that the solution $\bar{u}_j^n$ takes on the form of a single Fourier mode, we can write

$$\bar{u}_j^n = \exp\left[i\left(\kappa j h - \omega n \Delta t\right)\right],$$

which can be used in Eq. (36) to obtain the discrete dispersion relation between $\omega\Delta t$ and κh at a given CFL number μ. Since all terms in the left-hand side of Eq. (36) are considered at the same time step, the time component of the Fourier mode can be factored out, which gives rise to

$$\exp\left(-i\omega\Delta t\right) = 1 + Q_{\text{in}} - Q_{\text{out}},$$

or

$$\omega\Delta t = i \ln\left(1 + Q_{\text{in}} - Q_{\text{out}}\right), \tag{37}$$

where $\ln$ is the natural logarithm and Q_{in} and Q_{out} are the incoming and outgoing fluxes, respectively, expressed in terms of exponentials that translate the spatial dependence of the fluxes. The fluxes depend on the reconstruction polynomial and on the edge values and edge slopes. The algebra is tedious and Eq. (37) is solved using MATLAB. The real part of the solution is indicative of the phase error while the imaginary part gives information on the amount of numerical diffusion introduced by the discretization. Results are shown in Figure 11 for a CFL number of 0.25.

The best candidates are PPM ih_4 and PQM $ih6/ih6$, which introduce less numerical diffusion and exhibit better phase properties. PQM $ih4/ih4$ also has good properties but is only fourth-order accurate, which, as already mentioned, is considered wasteful in that PQM should at least be fifth-order accurate.

3.2 Numerical experiments

We now perform traditional advection experiments in a periodic domain, starting with the following initial condition, inspired by [5] :

$$f = \begin{cases} \exp\left[-\dfrac{(x-0.125)^2}{0.0003}\right] & \text{if} \quad 0.075 \le x \le 0.175, \\ 1 & \text{if} \quad 0.325 \le x \le 0.425, \\ 1 - 20|x - 0.625| & \text{if} \quad 0.575 \le x \le 0.675, \\ \left[1 - 400\left(x - 0.875\right)^2\right]^{1/2} & \text{if} \quad 0.825 \le x \le 0.925, \\ 0 & \text{otherwise.} \end{cases} \tag{38}$$

The unlimited versions of PPM and PQM are first used and the results are presented in Figure 12. The limited versions are then considered to run the advection test on uniform and nonuniform grids, with results shown in Figures 13 and 14, respectively. In all cases, the grid has 160 cells and results are presented after 10 revolutions. All experiments show that PQM schemes outperform PPM schemes, which is especially visible for the limited cases.

At low resolutions, the dispersion analysis suggests that PPM ih_4 would outperform PQM h_5/h_4 by being less diffusive, especially to resolve higher wavenumers (Figure 11). This property is confirmed in Figure 15. However, the advantage of PPM ih_4 over PQM h_5/h_4 is lost when the limited

versions of these schemes are used because both schemes yield similar results. In the limited cases, all PQM advection schemes perform better, all resolutions considered.

Similarly to the PQM limiter, the PPM limiter also operates in two phases. The first one guarantees boundedness of edge values using Eqs (19) and (20). The second phase enforces monotonicity by adjusting one of the edge values (see [4] for details on this phase) to shift the extremum, if any, onto an edge. Finally, extrema in the data set are represented by piecewise constants.

3.3 Convergence analysis

A convergence analysis is carried out on uniform grids for the advection of a Gaussian in a periodic domain. Results are shown in Figure 16 for a CFL number of 0.25 and after one revolution. The convergence rates are established with respect to the Euclidian norm, defined by

$$||e||_{\text{eucl}} = \left[\sum_{j=1}^{N} |\bar{u}_j - \bar{u}_{j,\text{EXACT}}|^2 \right]^{1/2}, \tag{39}$$

where $\bar{u}_{j,\text{EXACT}}$ is the exact average in cell j, as computed using the exact analytical solution. Note that the Euclidian norm is a better measure than the L_2 norm for computing advection errors since the objective is to evaluate how cell averages are transported by the advection scheme. In this respect, reconstruction is merely a means to achieve this objective.

For unlimited advection schemes, convergence rates are very similar to that obtained for the unlimited reconstruction schemes. In particular, it is noted that the PQM h_6/h_5 and ih_6/ih_6 schemes are both sixth-order accurate. At low resolution, PQM ih_4/ih_4 outperforms PQM h_5/h_4. This situation is reversed at higher resolution as the fourth-order accurate scheme is outpaced by the fifth-order accurate scheme. As was already the case for the reconstruction convergence analysis, convergence rates on nonuniform grids are roughly the same and are not shown. All limited schemes exhibit second-order accuracy because the global error is dominated by the first-order accuracy in the resolution of the Gaussian extremum. Since the grid size is divided by two at every step of the convergence analysis, this local error decreases by four, which yields second-order accuracy. However, this should not conceal the fact that, on a given grid, PQM schemes are globally more accurate (see Figures 13 - 15).

4 Treatment of boundaries

We now turn our attention on estimating the edge values and slopes at the boundaries. We limit our discussion to the following schemes: PPM h_4, PPM ih_4, PQM ih_4/ih_3 and PQM ih_6/ih_5, because they turn out to be the most effective. The concepts presented here are readily applicable to other schemes.

For PPM h_4, edge values are estimated by using fourth-order polynomials spanning four cells. Thus, this scheme is not directly applicable to the first and last two edges for which another approach must be considered. One possibility is to gradually decrease the order of accuracy of these estimates, down to a first-order estimate at the boundary where the edge value is taken to be equal to the boundary cell average. Another approach, which we advocate, is to resort to one-sided fourth-order polynomials so that the same order of accuracy is preserved throughout the domain. Hence, the first and last two edge values are estimated by using the polynomial spanning the first and last four cells, respectively. On uniform grids, the first and second one-sided, fourth-order edge-value estimates are

given by

$$\begin{aligned} u_1 &= \frac{1}{12}\left[25\bar{u}_1 - 23\bar{u}_2 + 13\bar{u}_3 - 3\bar{u}_4\right], \\ u_2 &= \frac{1}{12}\left[3\bar{u}_1 + 13\bar{u}_2 - 5\bar{u}_3 + \bar{u}_4\right]. \end{aligned} \tag{40}$$

Similarly, the last two edge-value estimates are given by (assuming the grid comprises N cells)

$$\begin{aligned} u_N &= \frac{1}{12}\left[\bar{u}_{N-3} - 5\bar{u}_{N-2} + 13\bar{u}_{N-1} + 3\bar{u}_N\right], \\ u_{N+1} &= \frac{1}{12}\left[-3\bar{u}_{N-3} + 13\bar{u}_{N-2} - 23\bar{u}_{N-1} + 25\bar{u}_N\right]. \end{aligned} \tag{41}$$

We note that, on nonuniform grids, these edge values are estimated by first computing the coefficients of the polynomials spanning the first and last four cells. These polynomials are then evaluated at the locations of the first and last three edges, respectively, to obtain the edge-value estimates. This approach is more computationally efficient than resorting to a closed-form expression such as Eq. (50) because once the polynomial is computed, it can be used three times. The coefficients of the polynomial are found by solving a linear system based on the relationships (8).

In addition to being more accurate and having better dispersion properties than PPM h_4, PPM ih_4 better handles boundaries because it uses a shorter stencil. In particular, the implicit relationship (13) – with $a = d = 0$ – can be written for both the second and second to last edges. Only the boundary edge values need to be prescribed in order for the tridiagonal system to be solvable. This is done by using the one-sided, fourth-order explicit estimates u_1 and u_{N+1}, as given by (40) and (41). Since all edge-value estimates are linked, the accuracy of the boundary edge-value estimates has an influence on all other interior estimates. Therefore, it is important to use a fourth-order scheme to estimate the boundary edge values (even though the accuracy of the edge-value estimates at the boundaries may be subsequently reduced by the limiter).

The boundary treatment for PQM ih_4/ih_3 is not different from that considered for PPM ih_4. In addition to prescribing the boundary edge values, we also need to prescribe the boundary edge slopes. These boundary conditions are enforced by using the same fourth-order accurate polynomial spanning four cells. The boundary edge value is computed by evaluating the polynomial at the boundary while the slope is computed by evaluating the derivative of the polynomial. For uniform grids, third-order boundary edge slopes are given by

$$\begin{aligned} u'_1 &= \frac{1}{12h}\left[-11\bar{u}_1 + 45\bar{u}_2 - 69\bar{u}_3 + 35\bar{u}_4\right], \\ u'_{N+1} &= \frac{1}{12h}\left[-35\bar{u}_{N-3} + 69\bar{u}_{N-2} - 45\bar{u}_{N-1} + 11\bar{u}_N\right]. \end{aligned} \tag{42}$$

The PQM ih_6/ih_5 scheme requires a little more work. Because the sixth-order implicit scheme (13) spans four cells, it can only be written for edges 3 to $N-1$ and sixth-order estimates must be provided for the first and last two edge values. We propose to use one-sided, sixth-order implicit schemes for the second and second to last edges and sixth-order explicit estimates at the boundaries to close the tridiagonal system. A left-sided implicit scheme can be written as

$$\alpha u_{j-\frac{1}{2}} + u_{j+\frac{1}{2}} + \beta u_{j+\frac{3}{2}} = a\bar{u}_j + b\bar{u}_{j+1} + c\bar{u}_{j+2} + d\bar{u}_{j+3}, \tag{43}$$

which is an expression between four cell averages and the three leftmost edge values of the stencil. Unlike Eq. (13), the above relationship can be written for the second edge value. Similarly, a right-sided implicit scheme is given by

$$\alpha u_{j-\frac{1}{2}} + u_{j+\frac{1}{2}} + \beta u_{j+\frac{3}{2}} = a\bar{u}_{j-2} + b\bar{u}_{j-1} + c\bar{u}_j + d\bar{u}_{j+1} \tag{44}$$

and expresses four cell averages in terms of the rightmost edge values of the stencil. It can be utilized with respect to the second to last edge value. The coefficients α, β, a, b, c and d of Eqs (43) and (44) are given in Table 3 for uniform grids and in the Appendix for nonuniform grids via the solutions to linear systems. As for the edge values, writing implicit relationships for the second and second to last edge slopes requires to resort to one-sided formulae, which are now presented. A left-sided implicit scheme can be written as

$$\alpha u'_{j-\frac{1}{2}} + u'_{j+\frac{1}{2}} + \beta u'_{j+\frac{3}{2}} = a\bar{u}_j + b\bar{u}_{j+1} + c\bar{u}_{j+2} + d\bar{u}_{j+3}, \tag{45}$$

which is an expression between four cell averages and the three leftmost edge slopes of the stencil. Similarly, a right-sided implicit scheme is given by

$$\alpha u'_{j-\frac{1}{2}} + u'_{j+\frac{1}{2}} + \beta u'_{j+\frac{3}{2}} = a\bar{u}_{j-2} + b\bar{u}_{j-1} + c\bar{u}_j + d\bar{u}_{j+1} \tag{46}$$

and expresses four cell averages in terms of the rightmost edge slopes of the stencil. The coefficients α, β, a, b, c and d of Eqs (45) and (46) are given in Table 4 for uniform grids and in the Appendix for nonuniform grids via the solutions to linear systems. The tridiagonal systems for the edge values and slopes are closed by prescribing the following sixth-order boundary edge values:

$$\begin{aligned} u_1 &= \frac{1}{720}\left[1764\bar{u}_1 - 2556\bar{u}_2 + 2844\bar{u}_3 - 1956\bar{u}_4 + 744\bar{u}_5 - 120\bar{u}_6\right], \\ u_{N+1} &= \frac{1}{720}\left[-120\bar{u}_{N-5} + 744\bar{u}_{N-4} - 1956\bar{u}_{N-3} + 2844\bar{u}_{N-2} - 2556\bar{u}_{N-1} + 1764\bar{u}_N\right], \end{aligned} \tag{47}$$

and fifth-order boundary edge slopes:

$$\begin{aligned} u'_1 &= \frac{1}{720h}\left[-3248\bar{u}_1 + 9280\bar{u}_2 - 11780\bar{u}_3 + 8540\bar{u}_4 - 3340\bar{u}_5 + 548\bar{u}_6\right], \\ u'_{N+1} &= \frac{1}{720h}\left[-548\bar{u}_{N-5} + 3340\bar{u}_{N-4} - 8540\bar{u}_{N-3} + 11780\bar{u}_{N-2} - 9280\bar{u}_{N-1} + 3248\bar{u}_N\right]. \end{aligned} \tag{48}$$

Expressions (47) and (48) are valid for uniform grids. On nonuniform grids, the coefficients of the boundary polynomials are first computed. The polynomials and their derivatives are then evaluated at the boundary to give the boundary edge values and slopes.

The order of accuracy of the boundary conditions has a nonnegligible influence on the overall quality of solutions to unlimited remapping experiments in a closed domain. In Figure 17, the reconstructed profiles are shown after 1000 remapping cycles. Each cycle comprises four steps: (i) reconstruction on grid A, (ii) remapping onto grid B (different than grid A and for each cycle), (iii) reconstruction on grid B and (iv) remapping back onto grid A. In Figure 17, grid A is a 20-cell uniform grid and grid B is an 18-cell nonuniform grid. For each experiment, the initial condition is a set of cell averages based on the exact profile. At each cycle, information is lost when grids A and B are different. The best schemes are those for which this loss is the smallest. The overall quality of the solutions is impaired when low-order boundary conditions are used. Low-order boundary conditions consist in setting the boundary edge values equal to the boundary cell averages and setting the boundary edge slopes equal to zero. This is equivalent to considering a constant approximation at the boundary. For PPM h_4, the second and second to last edge values are made equal to second-order estimates using adjacent cell averages. As a sanity check, it was verified that all PPM schemes could exactly (i.e., to machine accuracy) reproduce parabolas and that PQM ih_4/ih_3 and PQM ih_6/ih_5 could exactly reproduce cubics and quartics, respectively. In Figure 18, a convergence analysis is conducted for which the remapping experiments, as described above, are carried out on gradually finer grids. Using low-order boundary conditions reduces the order of accuracy of all schemes to 2.5 whereas high-order boundary conditions allow to preserve the nominal orders of accuracy.

5 Computational cost

The relative computational costs of PPM and PQM schemes are now briefly investigated on the basis of remapping experiments in closed domains, as described in Figure 17b (high-order boundary conditions are used). The errors and elapsed computational times are reported in Table 5 for unlimited and limited remapping experiments consisting of 20000 cycles between a uniform 100-cell grid and a nonuniform 90-cell grid. Both the unlimited and limited versions of PQM schemes are more cost-effective than their PPM counterparts. In particular, the error incurred by the unlimited PQM ih_6/ih_5 scheme is decreased by more than three orders of magnitude compared with PPM h_4 for only a 30% extra cost. The same tendency occurs for the limited versions of these schemes, although not as dramatically. Whereas the unlimited PPM h_4 scheme is cheaper than the unlimited PPM ih_4 scheme, the opposite is true for the limited versions of these schemes. That is, the limited PPM ih_4 scheme turns out to be cheaper than the limited PPM h_4 scheme (see Table 5). This originates from the fact that ih_4 edge-value estimates are more accurate than h_4 estimates and the limiter does not need to be activated as often with the former, making PPM ih_4 relatively less expensive. For the same reason, limited PQM schemes are not as expensive as unlimited PQM schemes, in relative terms.

Given a target error, Table 6 shows the grid resolution needed and computational times incurred to attain that error for different unlimited and limited schemes. The remapping experiment is the same as that described in Figure 17b. Note that different target errors are considered for the unlimited and limited cases. For a given error, PPM h_4 is almost five times more expensive than PQM ih_6/ih_5 for the unlimited versions of these schemes. The extra cost amounts to 10% for the limited versions.

6 Conclusion

We have presented a hierarchy of one-dimensional high-order remapping schemes and investigated their performance with respect to accuracy, convergence rate and dispersion. The schemes have also been compared based on traditional advection experiments in periodic domains and remapping experiments in closed domains. We have introduced the new PQM scheme that is based on fifth-order accurate piecewise quartics. A limiter for this scheme has been fully described that never decreases the polynomial degree, except at the location of extrema where piecewise constants are used. PPM has also been revisited and compared with PQM by using a series of high-order explicit and implicit (i.e., compact) estimates for the edge values and slopes, with significant improvements gained when using implicit estimates.

All analyses have been carried out in one dimension because our main focus is the improvement of vertical coordinate systems in hybrid ocean models. However, we believe that the material presented is also applicable to higher dimensions. In fact, the use of PPM advection schemes is not uncommon [e.g., 14] and, in that respect, some of the improvements presented in this paper could be directly used in existing algorithms.

Based on the analysis of computational costs, it is found that PQM ih_6/ih_5 is by far the most cost-effective scheme when it is unlimited and remains very advantageous when the limiter is activated. It is also shown that all limited PQM schemes perform significantly better than limited PPM schemes. Moreover, we note that the limited PQM scheme has room for improvement, and it would certainly benefit from state-of-the-art monotonicity-preserving limiters that are currently used for PPM schemes [e.g., 17].

A Estimates of edge values and slopes on nonuniform grids

Some estimates for edge values and slopes are now provided for nonuniform grids. Since not all schemes are recommended, we limit ourselves to PPM h_3, PPM h_4, PPM ih_4, PQM ih_4/ih_3 and PQM ih_6/ih_5.

A.1 Edge values

A.1.1 Explicit schemes

Third-order estimates are given by

$$\begin{aligned} u_{j-\frac{1}{2}} &= \frac{(h_1+h_2)(h_1\bar{u}_0+h_0\bar{u}_1)}{(h_0+h_1)(h_0+h_1+h_2)} + \frac{(2h_1+h_2)h_0\bar{u}_1 - h_0h_1\bar{u}_2}{(h_1+h_2)(h_0+h_1+h_2)}, \\ u_{j+\frac{1}{2}} &= \frac{(h_0+2h_1)h_2\bar{u}_1 - h_1h_2\bar{u}_0}{(h_0+h_1)(h_0+h_1+h_2)} + \frac{(h_0+h_1)(h_2\bar{u}_1+h_1\bar{u}_2)}{(h_1+h_2)(h_0+h_1+h_2)}, \end{aligned} \tag{49}$$

where $\bar{u}_0 = \bar{u}_{j-1}$, $\bar{u}_1 = \bar{u}_j$, $\bar{u}_2 = \bar{u}_{j+1}$ and $h_0 = h_{j-1}$, $h_1 = h_j$, $h_2 = h_{j+1}$.

Fourth-order estimates are given by

$$\begin{aligned} u_{j-\frac{1}{2}} = \; & \frac{1}{h_0+h_1+h_2+h_3}\times \\ & \left\{ \frac{(h_0+h_1)(h_2+h_3)}{(h_1+h_2)}(\bar{u}_1h_2+\bar{u}_2h_1)\left(\frac{1}{h_0+h_1+h_2}+\frac{1}{h_1+h_2+h_3}\right)\right. \\ & + \frac{h_2(h_2+h_3)}{(h_0+h_1+h_2)(h_0+h_1)}\left[\bar{u}_1(h_0+2h_1)-\bar{u}_0h_1\right] \\ & \left. + \frac{h_1(h_0+h_1)}{(h_1+h_2+h_3)(h_2+h_3)}\left[\bar{u}_2(2h_2+h_3)-\bar{u}_3h_2\right]\right\} \end{aligned} \tag{50}$$

where $\bar{u}_0 = \bar{u}_{j-2}$, $\bar{u}_1 = \bar{u}_{j-1}$, $\bar{u}_2 = \bar{u}_j$, $\bar{u}_3 = \bar{u}_{j+1}$ and $h_0 = h_{j-2}$, $h_1 = h_{j-1}$, $h_2 = h_j$, $h_3 = h_{j+1}$. The right-hand side edge value, $u_{j+\frac{1}{2}}$, is simply obtained by translating the index to the right by one unit.

A.1.2 Implicit schemes

The coefficients in Eq. (13) for the fourth-order estimates are given by

$$\begin{aligned} \alpha &= \frac{h_1^2}{(h_0+h_1)^2}, \\ \beta &= \frac{h_0^2}{(h_0+h_1)^2}, \\ a &= 0, \\ b &= 2h_1^2\frac{h_1^2+2h_0^2+3h_0h_1}{(h_0+h_1)^4}, \\ c &= 2h_0^2\frac{h_0^2+2h_1^2+3h_0h_1}{(h_0+h_1)^4}, \\ d &= 0, \end{aligned} \tag{51}$$

where $h_0 = h_j$, $h_1 = h_{j+1}$. It turns out that computing the coefficients (51) has a cost of 36 multiplications and 8 additions. Alternatively, we might as well compute the coefficients by solving the following linear system

$$\begin{bmatrix} 1 & 1 & -1 & -1 \\ -2h_0 & 2h_1 & h_0 & h_1 \\ 3h_0^2 & 3h_1^2 & -h_0^2 & -h_1^2 \\ -4h_0^3 & 4h_1^3 & h_0^3 & -h_1^3 \end{bmatrix} \begin{bmatrix} \alpha \\ \beta \\ b \\ c \end{bmatrix} = \begin{bmatrix} -1 \\ 0 \\ 0 \\ 0 \end{bmatrix}, \tag{52}$$

which has a cost of 36 multiplications and 26 additions to solve the system, assuming that a standard Gaussian elimination is used. This is in addition to the cost of setting up the system. So, there is no clear computational advantage in using the closed-form expressions. As the order of accuracy increases, it becomes computationally cheaper to calculate the coefficients of the implicit scheme by solving a linear system. In addition, algebraic manipulations involved in the computation of closed-form solutions become quickly intractable.

The coefficients in Eq. (13) for the implicit sixth-order estimates are given by the solution to the following linear system:

$$\begin{bmatrix} 1 & 1 & -1 & -1 & -1 & -1 \\ -2h_1 & 2h_2 & -\Delta_2 & h_1 & -h_2 & -\nabla_2 \\ 3h_1^2 & 3h_2^2 & \Delta_3 & -h_1^2 & -h_2^2 & -\nabla_3 \\ -4h_1^3 & 4h_2^3 & -\Delta_4 & h_1^3 & -h_2^3 & -\nabla_4 \\ 5h_1^4 & 5h_2^4 & \Delta_5 & -h_1^4 & -h_2^4 & -\nabla_5 \\ -6h_1^5 & 6h_2^5 & -\Delta_6 & h_1^5 & -h_2^5 & -\nabla_6 \end{bmatrix} \begin{bmatrix} \alpha \\ \beta \\ a \\ b \\ c \\ d \end{bmatrix} = \begin{bmatrix} -1 \\ 0 \\ 0 \\ 0 \\ 0 \\ 0 \end{bmatrix}, \tag{53}$$

where

$$\begin{aligned} \Delta_k &= \frac{h_1^k - (h_0 + h_1)^k}{h_0}, \\ \nabla_k &= \frac{(h_2 + h_3)^k - h_2^k}{h_3}, \end{aligned}$$

with $h_0 = h_{j-1}$, $h_1 = h_j$, $h_2 = h_{j+1}$, $h_3 = h_{j+2}$.

The coefficients in Eq. (43) for the left-sided, implicit sixth-order estimates are given by the solution to the following linear system:

$$\begin{bmatrix} 1 & 1 & -1 & -1 & -1 & -1 \\ -2(h_0+h_1) & 0 & -\Delta_2 & h_1 & -h_2 & -\nabla_2 \\ 3(h_0+h_1)^2 & 0 & \Delta_3 & -h_1^2 & -h_2^2 & -\nabla_3 \\ -4(h_0+h_1)^3 & 0 & -\Delta_4 & h_1^3 & -h_2^3 & -\nabla_4 \\ 5(h_0+h_1)^4 & 0 & \Delta_5 & -h_1^4 & -h_2^4 & -\nabla_5 \\ -6(h_0+h_1)^5 & 0 & -\Delta_6 & h_1^5 & -h_2^5 & -\nabla_6 \end{bmatrix} \begin{bmatrix} \alpha \\ \beta \\ a \\ b \\ c \\ d \end{bmatrix} = \begin{bmatrix} -1 \\ 2h_1 \\ -3h_1^2 \\ 4h_1^3 \\ -5h_1^4 \\ 6h_1^5 \end{bmatrix}, \tag{54}$$

where

$$\begin{aligned} \Delta_k &= \frac{h_1^k - (h_0 + h_1)^k}{h_0}, \\ \nabla_k &= \frac{(h_2 + h_3)^k - h_2^k}{h_3}, \end{aligned}$$

with $h_0 = h_j$, $h_1 = h_{j+1}$, $h_2 = h_{j+2}$, $h_3 = h_{j+3}$.

The coefficients in Eq. (44) for the right-sided, implicit sixth-order estimates are given by the solution to the following linear system:

$$\begin{bmatrix} 1 & 1 & -1 & -1 & -1 & -1 \\ 0 & 2(h_2+h_3) & -\Delta_2 & h_1 & -h_2 & -\nabla_2 \\ 0 & 3(h_2+h_3)^2 & \Delta_3 & -h_1^2 & -h_2^2 & -\nabla_3 \\ 0 & 4(h_2+h_3)^3 & -\Delta_4 & h_1^3 & -h_2^3 & -\nabla_4 \\ 0 & 5(h_2+h_3)^4 & \Delta_5 & -h_1^4 & -h_2^4 & -\nabla_5 \\ 0 & 6(h_2+h_3)^5 & -\Delta_6 & h_1^5 & -h_2^5 & -\nabla_6 \end{bmatrix} \begin{bmatrix} \alpha \\ \beta \\ a \\ b \\ c \\ d \end{bmatrix} = \begin{bmatrix} -1 \\ -2h_2 \\ -3h_2^2 \\ -4h_2^3 \\ -5h_2^4 \\ -6h_2^5 \end{bmatrix}, \tag{55}$$

where

$$\begin{aligned} \Delta_k &= \frac{h_1^k - (h_0+h_1)^k}{h_0}, \\ \nabla_k &= \frac{(h_2+h_3)^k - h_2^k}{h_3}, \end{aligned}$$

with $h_0 = h_{j-2}$, $h_1 = h_{j-1}$, $h_2 = h_j$, $h_3 = h_{j+1}$.

A.2 Edge slopes

The coefficients in Eq. (16) for the implicit third-order estimates are given by

$$\begin{aligned} \alpha &= \frac{h_1\left(h_0^2 + h_0h_1 - h_1^2\right)}{(h_0+h_1)\left[(h_0+h_1)^2 + h_0h_1\right]}, \\ \beta &= \frac{h_0\left(h_1^2 + h_0h_1 - h_0^2\right)}{(h_0+h_1)\left[(h_0+h_1)^2 + h_0h_1\right]}, \\ a &= 0, \\ b &= \frac{-12h_0h_1}{(h_0+h_1)\left[(h_0+h_1)^2 + h_0h_1\right]}, \\ c &= \frac{12h_0h_1}{(h_0+h_1)\left[(h_0+h_1)^2 + h_0h_1\right]}, \\ d &= 0, \end{aligned} \tag{56}$$

where $h_0 = h_j$, $h_1 = h_{j+1}$.

The coefficients in Eq. (16) for the implicit fifth-order estimates are given by the solution to the following linear system:

$$\begin{bmatrix} 0 & 0 & 1 & 1 & 1 & 1 \\ 2 & 2 & -\Delta_2 & h_1 & -h_2 & -\nabla_2 \\ 6h_1 & -6h_2 & -\Delta_3 & h_1^2 & h_2^2 & \nabla_3 \\ -12h_1^2 & -12h_2^2 & \Delta_4 & -h_1^3 & h_2^3 & \nabla_4 \\ 20h_1^3 & -20h_2^3 & -\Delta_5 & h_1^4 & h_2^4 & \nabla_5 \\ -30h_1^4 & -30h_2^4 & \Delta_6 & -h_1^5 & h_2^5 & \nabla_6 \end{bmatrix} \begin{bmatrix} \alpha \\ \beta \\ a \\ b \\ c \\ d \end{bmatrix} = \begin{bmatrix} 0 \\ -1 \\ 0 \\ 0 \\ 0 \\ 0 \end{bmatrix}, \tag{57}$$

where

$$\begin{aligned}\Delta_k &= \frac{h_1^k - (h_0 + h_1)^k}{h_0}, \\ \nabla_k &= \frac{(h_2 + h_3)^k - h_2^k}{h_3},\end{aligned}$$

with $h_0 = h_{j-1}$, $h_1 = h_j$, $h_2 = h_{j+1}$, $h_3 = h_{j+2}$.

The coefficients in Eq. (45) for the left-sided, implicit fifth-order estimates are given by the solution to the following linear system:

$$\begin{bmatrix} 0 & 0 & 1 & 1 & 1 & 1 \\ 2 & 2 & -\Delta_2 & h_1 & -h_2 & -\nabla_2 \\ 6(h_0+h_1) & 0 & -\Delta_3 & h_1^2 & h_2^2 & \nabla_3 \\ -12(h_0+h_1)^2 & 0 & \Delta_4 & -h_1^3 & h_2^3 & \nabla_4 \\ 20(h_0+h_1)^3 & 0 & -\Delta_5 & h_1^4 & h_2^4 & \nabla_5 \\ -30(h_0+h_1)^4 & 0 & \Delta_6 & -h_1^5 & h_2^5 & \nabla_6 \end{bmatrix} \begin{bmatrix} \alpha \\ \beta \\ a \\ b \\ c \\ d \end{bmatrix} = \begin{bmatrix} 0 \\ -1 \\ -6h_1 \\ 12h_1^2 \\ -20h_1^3 \\ 30h_1^4 \end{bmatrix}, \tag{58}$$

where

$$\begin{aligned}\Delta_k &= \frac{h_1^k - (h_0 + h_1)^k}{h_0}, \\ \nabla_k &= \frac{(h_2 + h_3)^k - h_2^k}{h_3},\end{aligned}$$

with $h_0 = h_j$, $h_1 = h_{j+1}$, $h_2 = h_{j+2}$, $h_3 = h_{j+3}$.

The coefficients in Eq. (46) for the right-sided, implicit fifth-order estimates are given by the solution to the following linear system:

$$\begin{bmatrix} 0 & 0 & 1 & 1 & 1 & 1 \\ 2 & 2 & -\Delta_2 & h_1 & -h_2 & -\nabla_2 \\ 0 & -6(h_2+h_3) & -\Delta_3 & h_1^2 & h_2^2 & \nabla_3 \\ 0 & -12(h_2+h_3)^2 & \Delta_4 & -h_1^3 & h_2^3 & \nabla_4 \\ 0 & -20(h_2+h_3)^3 & -\Delta_5 & h_1^4 & h_2^4 & \nabla_5 \\ 0 & -30(h_2+h_3)^4 & \Delta_6 & -h_1^5 & h_2^5 & \nabla_6 \end{bmatrix} \begin{bmatrix} \alpha \\ \beta \\ a \\ b \\ c \\ d \end{bmatrix} = \begin{bmatrix} 0 \\ -1 \\ 6h_2 \\ 12h_2^2 \\ 20h_2^3 \\ 30h_2^4 \end{bmatrix}, \tag{59}$$

where

$$\begin{aligned}\Delta_k &= \frac{h_1^k - (h_0 + h_1)^k}{h_0}, \\ \nabla_k &= \frac{(h_2 + h_3)^k - h_2^k}{h_3},\end{aligned}$$

with $h_0 = h_{j-2}$, $h_1 = h_{j-1}$, $h_2 = h_j$, $h_3 = h_{j+1}$.

Acknowledgments

We thank Bob Hallberg and Steve Griffies for comments regarding the topics covered in this paper. We also thank two anonymous reviewers for valuable suggestions that helped improve the manuscript. Laurent White is supported by the ECCO II project, "Estimating the Circulation and Climate of the Ocean: High Resolution Global-Ocean and Sea-Ice Reanalysis", NASA award number NNG06GC28G. Laurent White is an honorary postdoctoral researcher with the Belgian National Fund for Scientific Research (FNRS).

References

[1] C. N. Barron, A. B. Kara, P. J. Martin, R. C. Rhodes, and L. F. Smedstad. Formulation, implementation and examination of vertical coordinate choices in the Global Navy Coastal Ocean Model (NCOM). *Ocean Model.*, 11:347–375, 2006.

[2] R. Bleck. An oceanic general circulation model framed in hybrid isopycnic-Cartesian coordinates. *Ocean Model.*, 4(1):55–88, 2002.

[3] R. L. Carpenter, K. K. Droegemeier, P. R. Woodward, and C. E. Hane. Application of the piecewise parabolic method (ppm) to meteorological modeling. *Mon. Wea. Rev.*, 118:586–612, 1990.

[4] P. Colella and P. R. Woodward. The piecewise parabolic method (ppm) for gas-dynamical simulations. *J. Comput. Phys.*, 54:174–201, 1984.

[5] V. Daru and C. Tenaud. High order one-step monotonicity-preserving schemes for unsteady compressible flow calculations. *J. Comput. Phys.*, 193:563–594, 2004.

[6] G. R. Halliwell. Evaluation of vertical coordinate and vertical mixing algorithms in the HYbrid-Coordinate Ocean Model (HYCOM). *Ocean Model.*, 7:285–322, 2004.

[7] H. T. Huynh. Schemes and constraints for advection. In *Proceedings of the Fifteenth International Conference on Numerical Methods in Fluid Dynamics, Monterey, Ca, USA, 24-28 June 1996*, 1996.

[8] C. Lacor, S. Smirnov, and M. Baelmans. A finite volume formulation of compact central schemes on arbitrary structured grids. *J. Comput. Phys.*, 198:535–566, 2004.

[9] R. J. Leveque. *Finite volume methods for hyperbolic problems*. Cambridge University Press, 2002.

[10] S.-J. Lin. A vertically Lagrangian finite-volume dynamical core for global models. *Mon. Wea. Rev.*, 132:2293–2307, 2004.

[11] S.-J. Lin, W. C. Chao, Y. C. Sud, and G. K. Walker. A class of the van Leer transport schemes and its applications to the moisture transport in a general circulation model. *Mon. Wea. Rev.*, 122:1575–1593, 1994.

[12] L. G. Margolin and M. Shashkov. Second-order sign-preserving conservative interpolation (remapping) on general grids. *J. Comput. Phys.*, 184:266–298, 2003.

[13] J. Morrell, P. Sweby, and A. Barlow. A cell by cell anisotropic adaptive mesh ALE scheme for the numerical solution of the Euler equations. *J. Comput. Phys.*, 226:1152–1180, 2007.

[14] J. Pietrzak. The use of TVD limiters for forward-in-time upstream-biased advection schemes in ocean modeling. *Mon. Wea. Rev.*, 126:812–830, 1998.

[15] P. S. Schopf and A. Loughe. A reduced-gravity isopycnal ocean model: hindcasts of El Niño. *Mon. Wea. Rev.*, 123:28392863, 1995.

[16] M. Shashkov and B. Wendroff. The repair paradigm and application to conservation laws. *J. Comput. Phys.*, 198:265–277, 2004.

[17] A. Suresh and H. T. Huynh. Accurate monotonicity-preserving schemes with Runge-Kutta time stepping. *J. Comput. Phys.*, 136:83–99, 1997.

[18] B. van Leer. Towards the ultimate conservative difference scheme. V. A second-order sequel to Godunov's method. *J. Comput. Phys.*, 32(1):101–136, 1979.

[19] F. Xiao, T. Yabe, X. Peng, and H. Kobayashi. Conservative and oscillation-less atmospheric transport schemes based on rational functions. *J. Geophys. Res.*, 107:4609–4619, 2002.

[20] M. Zerroukat, N. Wood, and A. Staniforth. The Parabolic Spline Method (PSM) for conservative transport problems. *Int. J. Numer. Methods Fluids*, 51:1297–1318, 2006.

List of Tables

List of Figures

Order of accuracy	α	β	a	b	c	d
4 (ih_4)	$\frac{1}{4}$	$\frac{1}{4}$	0	$\frac{3}{4}$	$\frac{3}{4}$	0
5 (ih_5)	$\frac{1}{2}$	$\frac{1}{6}$	$\frac{1}{18}$	$\frac{19}{18}$	$\frac{5}{9}$	0
6 (ih_6)	$\frac{1}{12}$	$\frac{1}{12}$	$\frac{1}{36}$	$\frac{29}{36}$	$\frac{29}{36}$	$\frac{1}{36}$

Table 1: Coefficients to use in Eq. (13) giving implicit edge-value estimates on uniform grids.

Order of accuracy	α	β	a	b	c	d
4 (ih_4)	$\frac{1}{10}$	$\frac{1}{10}$	0	$-\frac{6}{5h}$	$\frac{6}{5h}$	0
6 (ih_6)	$\frac{2}{11}$	$\frac{2}{11}$	$-\frac{3}{44h}$	$-\frac{51}{44h}$	$\frac{51}{44h}$	$\frac{3}{44h}$

Table 2: Coefficients to use in Eq. (16) giving implicit edge-slope estimates on uniform grids.

Scheme	α	β	a	b	c	d
Left-sided, Eq. (43)	$\frac{1}{8}$	$\frac{3}{4}$	$\frac{43}{96}$	$\frac{123}{96}$	$\frac{15}{96}$	$-\frac{1}{96}$
Right-sided, Eq. (44)	$\frac{3}{4}$	$\frac{1}{8}$	$-\frac{1}{96}$	$\frac{15}{96}$	$\frac{123}{96}$	$\frac{43}{96}$

Table 3: Coefficients to use in Eqs (43) and (44) giving one-sided, sixth-order implicit edge-value estimates on uniform grids.

Scheme	α	β	a	b	c	d
Left-sided, Eq. (45)	$\frac{1}{10}$	$-\frac{7}{20}$	$-\frac{99}{80h}$	$\frac{141}{80h}$	$-\frac{45}{80h}$	$\frac{3}{80h}$
Right-sided, Eq. (46)	$-\frac{7}{20}$	$\frac{1}{10}$	$-\frac{3}{80h}$	$\frac{45}{80h}$	$-\frac{141}{80h}$	$\frac{99}{80h}$

Table 4: Coefficients to use in Eqs (45) and (46) giving one-sided, sixth-order implicit edge-slope estimates on uniform grids.

	Unlimited		Limited	
	Error	CPU time	Error	CPU time
PPM h_4	4.915566×10^{-3}	1.00	2.119396×10^{-2}	1.00
PPM ih_4	4.978881×10^{-3}	1.06	1.876330×10^{-2}	0.95
PQM ih_4/ih_3	2.621667×10^{-4}	1.17	1.224886×10^{-2}	1.01
PQM ih_6/ih_5	3.606455×10^{-6}	1.30	1.017189×10^{-2}	1.13

Table 5: Errors (L_2-norm) and computational times (relative to PPM h_4) for unlimited and limited remapping experiments in a closed domain (as described in Figure 17b). For each run, 20000 remapping cycles are carried out between a uniform grid comprising 100 cells and a nonuniform grid comprising 90 cells. The unlimited and limited PPM h_4 real computational times are 69 s and 76 s, respectively.

	Unlimited		Limited	
	Resolution	CPU time	Resolution	CPU time
PPM h_4	280	4.77	60	1.09
PPM ih_4	300	4.82	60	1.00
PQM ih_4/ih_3	125	5.68	50	0.95
PQM ih_6/ih_5	50	1.00	50	1.00

Table 6: Resolution needed and computational time incurred to roughly match the error (L_2-norm) obtained with PQM $ih6/ih5$ for a remapping experiment (as described in Figure 17b) in a closed domain consisting of 10000 remapping cycles. Each cycle is carried out between a uniform grid and a nonuniform grid whose number of cells is decreased by 10% relative to the uniform grid.

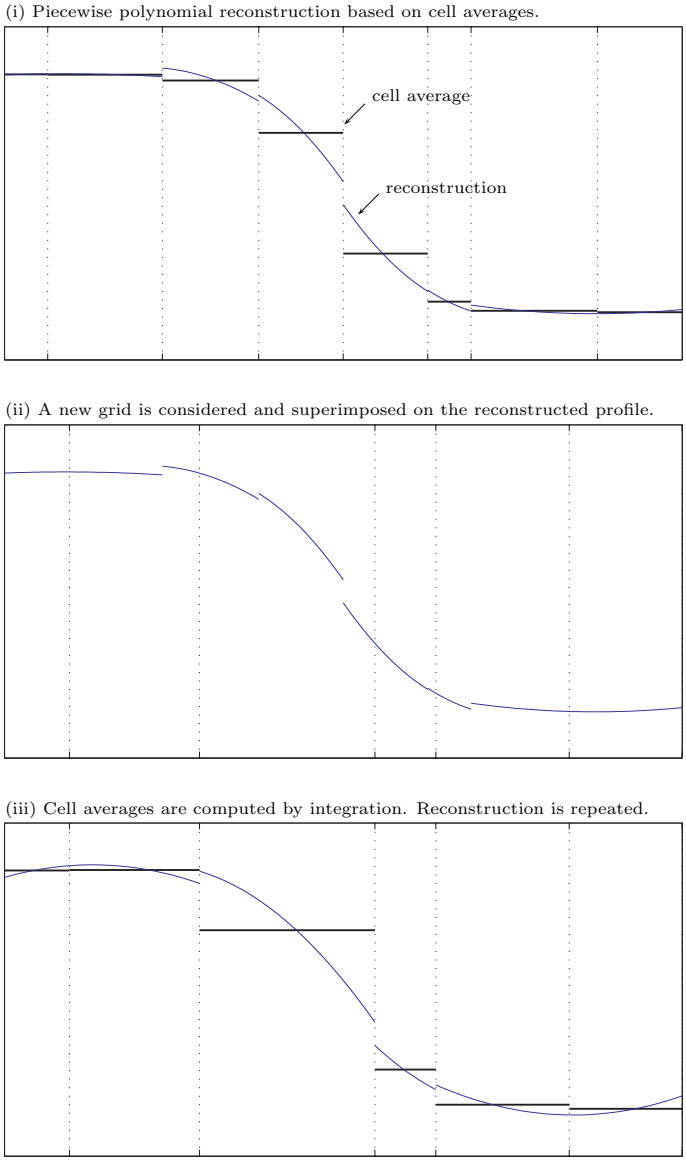

Figure 1: A regridding-remapping algorithm occurs in three steps. (i) Piecewise polynomial reconstruction based on cell averages on a given grid. (ii) A new grid is considered and superimposed on the reconstructed profile. (iii) Analytical integration of the reconstructed profile over the cells of the new grid allows to compute the cell averages for this new grid. The reconstruction step is then repeated. This illustration depicts the general case of reconstructions on nonuniform grids featuring discontinuities across cell interfaces.

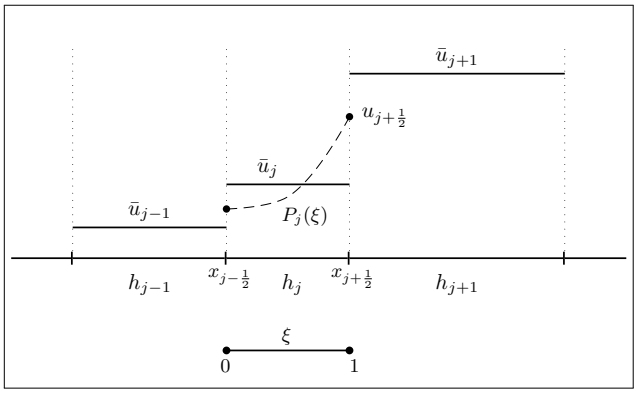

Figure 2: The average over cell j of width h_j is noted $\bar{u}_j$. For convenience, the mapping of $x \in [x_{j-\frac{1}{2}}, x_{j+\frac{1}{2}}]$ onto $\xi \in [0, 1]$ is used within each cell. The local polynomial reconstruction $P_j(\xi)$ is represented by the dashed line. Variables at cell interfaces are identified by half-integer indexes, such as the edge value $u_{j+\frac{1}{2}}$.

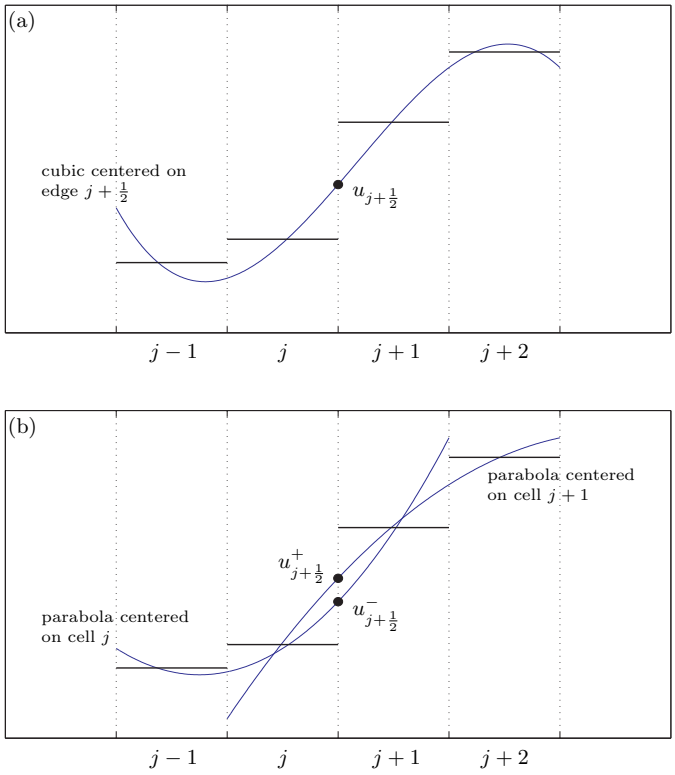

Figure 3: Explicit estimates for the edge value $u_{j+\frac{1}{2}}$ using (a) an even-order accurate edge-centered cubic spanning four cells and (b) two odd-order accurate cell-centered parabolas spanning three cells. Because the parabolas are cell-centered, they provide two different estimates for the edge value, $u^-_{j+\frac{1}{2}}$ and $u^+_{j+\frac{1}{2}}$, leading to a discontinuous reconstruction.

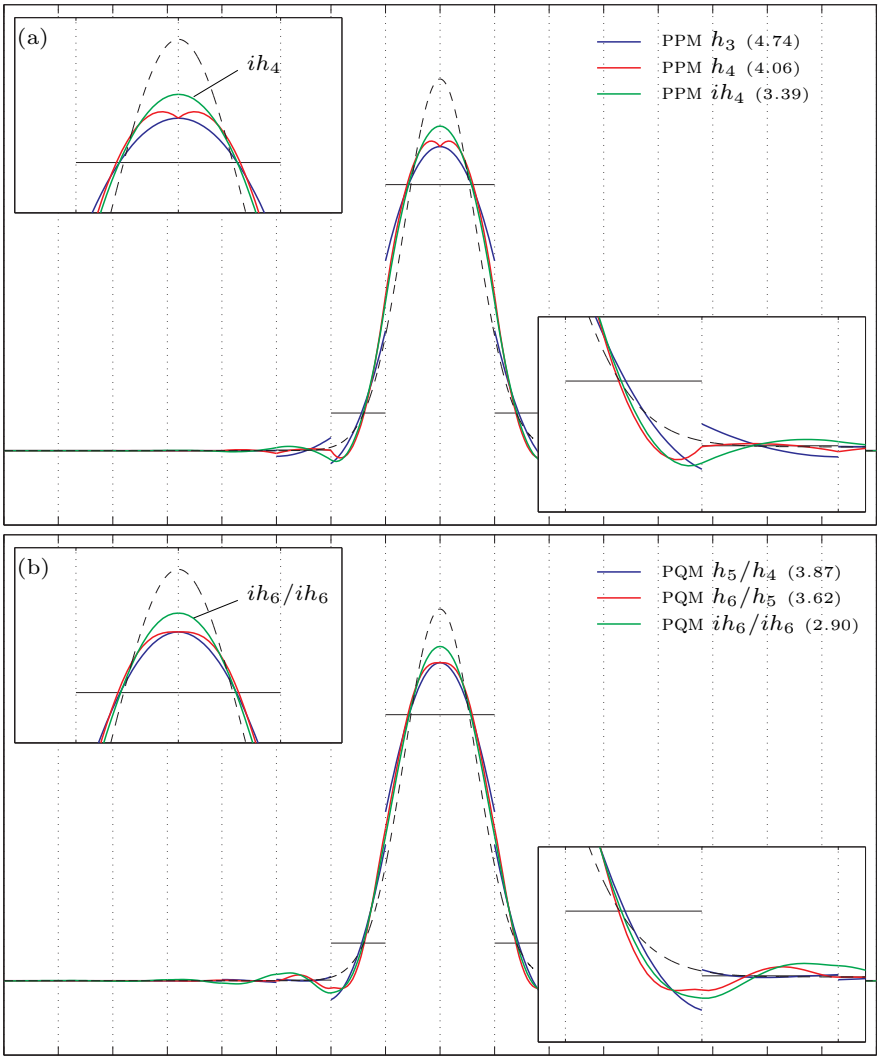

Figure 4: Reconstructions of a Gaussian on a periodic domain using (a) PPM with three different edge-value estimates and (b) PQM with three different edge-value estimates. The dashed line is the exact profile and cell averages are depicted by horizontal solid lines. The L_2-norms of the error ($\times 10^2$) are indicated in the legend, besides their respective schemes. In both cases, implicit estimates outperform their explicit equivalent, both visually and by comparing the norms. The implicit PPM ih_4 yields a lower error than both explicit PQM schemes.

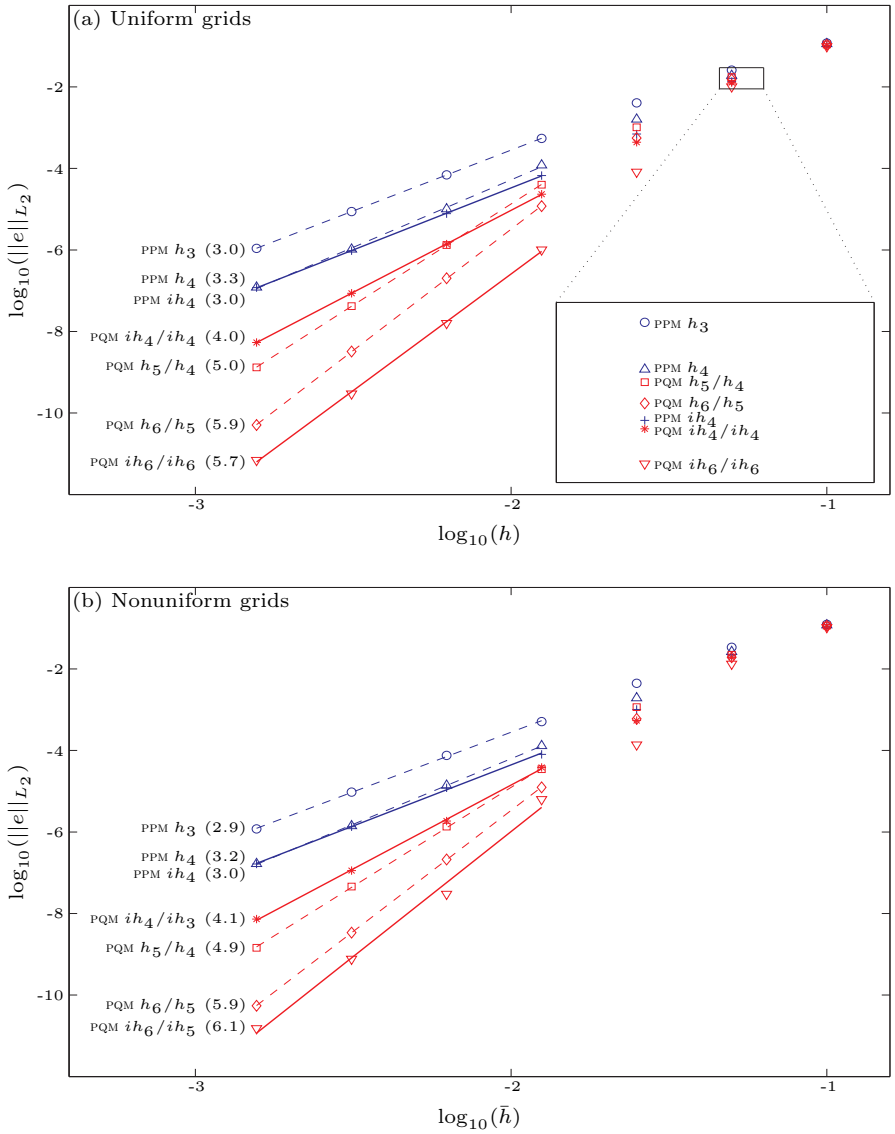

Figure 5: Orders of accuracy of reconstruction schemes for a Gaussian on (a) uniform grids and (b) random nonuniform grids. Convergence rates are given next to the scheme name, between parentheses. Random nonuniform grids are modified uniform grids for which all edge locations are perturbed by a uniformly-distributed number in $[-h/4, h/4]$, where h is the uniform grid size. Blue and red least-square linear curves are for PPM and PQM schemes, respectively. Dashed and solid lines are for explicit and implicit schemes, respectively. Whatever grid type is considered, PPM and PQM are at least third- and fifth-order accurate, respectively, when the order of accuracy for the edge-value and edge-slope estimates is high enough. At low resolution, PPM ih_4 turns out to be an excellent candidate, outperformed only by PQM $ih4/ih4$ and PQM $ih6/ih6$ – see inset on panel (a). PQM $ih4/ih4$, however, is only fourth-order accurate.

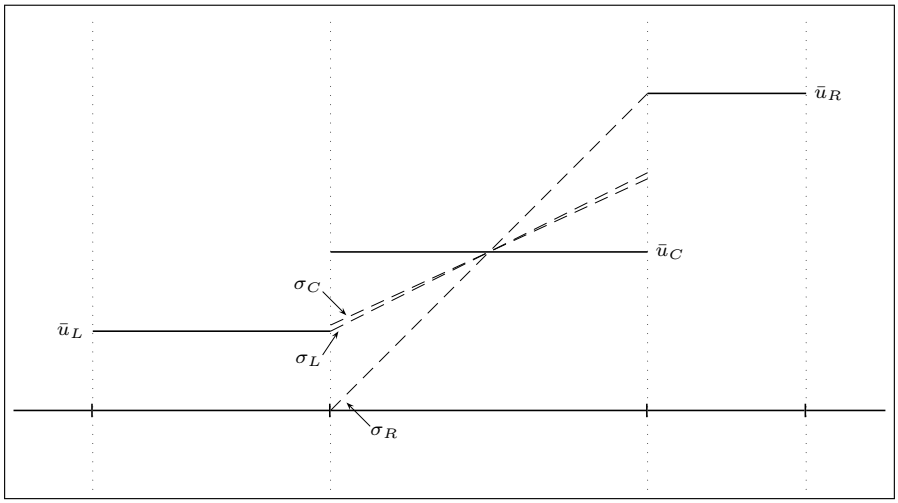

Figure 6: One-sided and centered slopes, as defined by Eq. (18). According to Eq. (17), the limited PLM slope is the centered one, σ_C, which serves as reference for the slope consistency checks in the limited PQM algorithm.

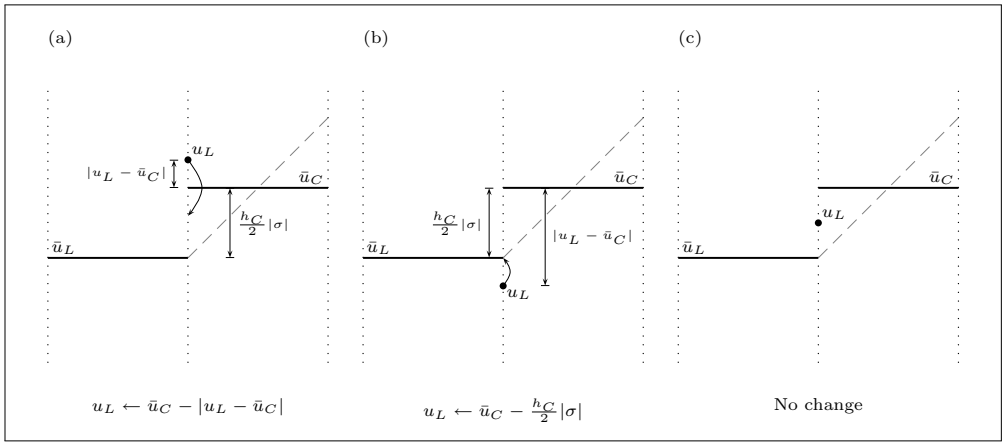

Figure 7: Estimations of edge values may be unbounded and, therefore, need to be limited to lie in the range defined by neighboring cell averages. The above example shows how a left edge value is limited using Eq. (19). The dashed line represents the PLM reconstruction based on the limited PLM slope σ. (a-b) The left edge value is unbounded and the minimum between $|u_L - \bar{u}_C|$ and $\frac{h_C}{2}|\sigma|$ is used to modify the edge value. (c) The estimate is bounded and is not modified. The distance $\frac{h_C}{2}|\sigma|$ is the absolute difference between the cell average $\bar{u}_C$ and the value of the PLM reconstruction at either cell edge.

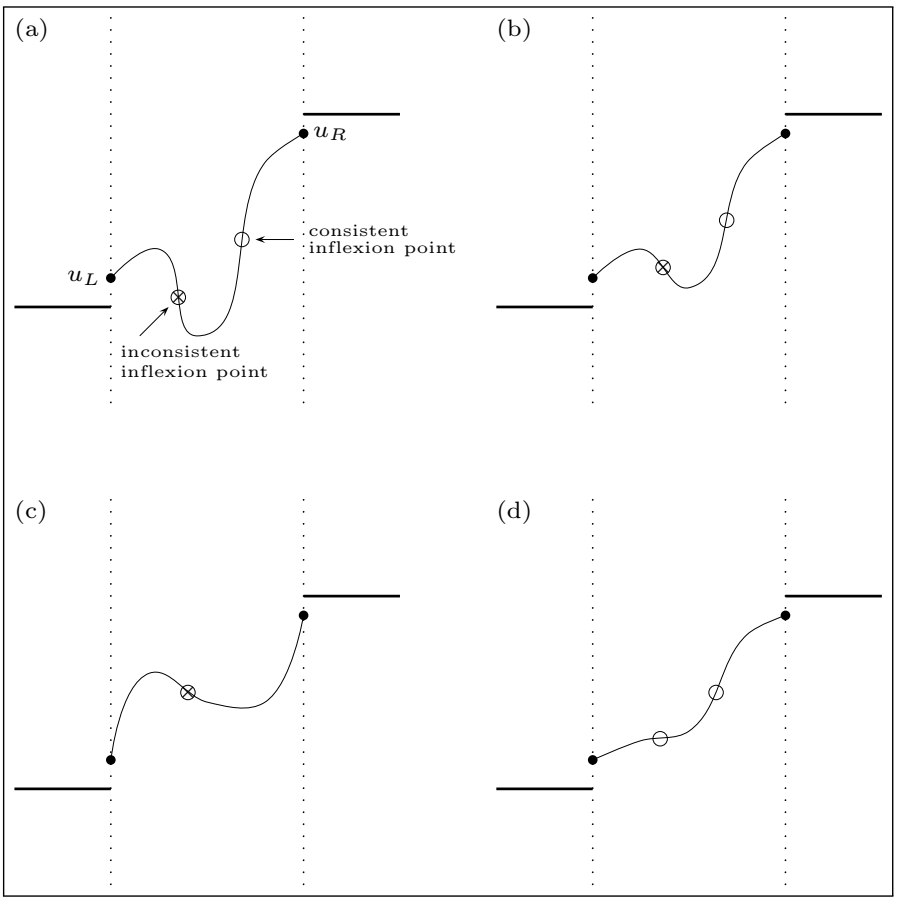

Figure 8: Examples of quartics that can be built based on bounded edge values and consistent edge slopes. The limited PLM slope σ is assumed to be positive, as are the edge slopes. (a) The quartic is neither monotonic nor bounded by neighboring cell averages. It features two inflexion points, one of which is inconsistent with respect to σ. (b) The quartic is nonmonotonic but is bounded and it also has two inflexion points, one of them being inconsistent. (c) The quartic is nonmonotonic and bounded. It has one inconsistent inflexion point. (d) The quartic is monotonic, bounded and it has two consistent inflexion points. Reconstructed quartics (a-c) are not acceptable while quartic (d) is acceptable.

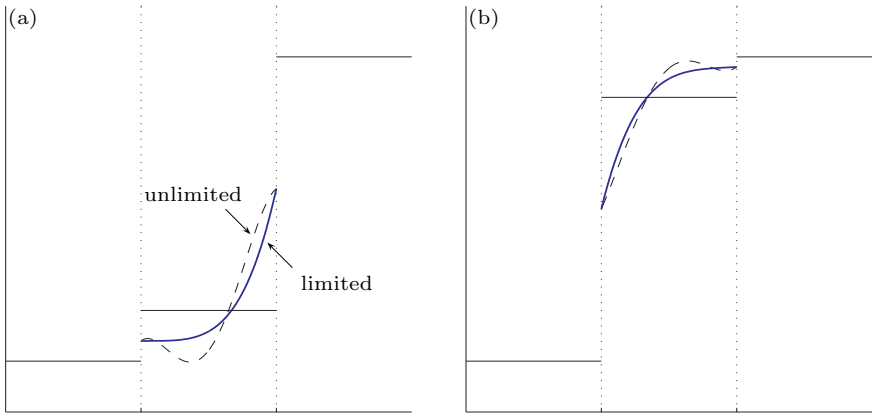

Figure 9: Dashed and solid curves are unlimited and limited quartics, respectively. Cell averages are represented by horizontal lines spanning the entire cell. Limiting is conducted by enforcing both inflexion points to collapse on one of the edges. This is done by adjusting the edge slopes. (a) Inflexion points are located on the left edge. Curvature is positive, which is the only possibility that does not violate local conservation (the quartic average must be equal to the cell average). (b) Inflexion points are located on the right edge. Curvature is negative. In both examples, the unlimited quartics have bounded edge values and consistent edge slopes (positive). Yet, they have inconsistent inflexion points.

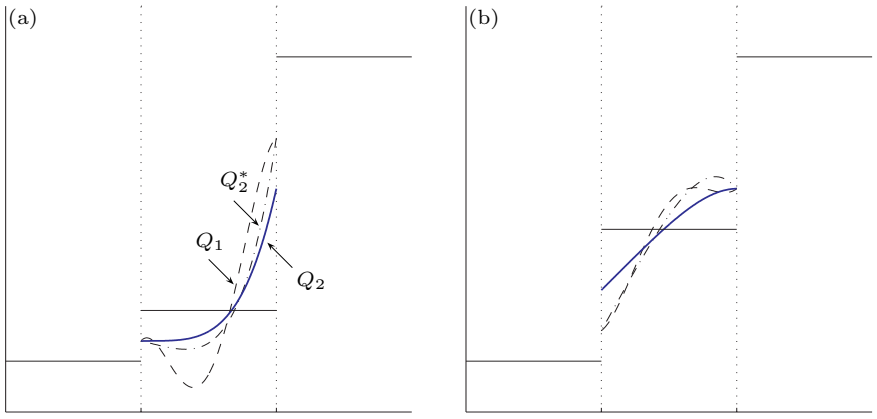

Figure 10: In both examples, the quartic Q_1 obtained after the first step of the limiting algorithm is nonmonotonic but the edge values are bounded and the edge slopes are consistent. The second step of the algorithm guarantees monotonicity by having both inflexion points collapse onto one of the edges (the left edge in these examples). A first-attempt quartic Q_2^* is produced that has a single-signed curvature, which is done by adjusting the edge slopes via (26)-(27) (or via (31)-(32) when inflexion points are located on the right edge). If one of the adjusted edge slopes is inconsistent, it is necessary to adjust the opposite edge value to obtain the definitive monotonic quartic Q_2. (a) The first-attempt quartic Q_2^* has an inconsistent left slope. Monotonicity is restored by setting the slope to zero and adjusting the right edge value, which produces the quartic Q_2. (b) Q_2^* has an inconsistent right slope. The monotonic quartic Q_2 is obtained by setting this slope to zero and adjusting the left edge value.

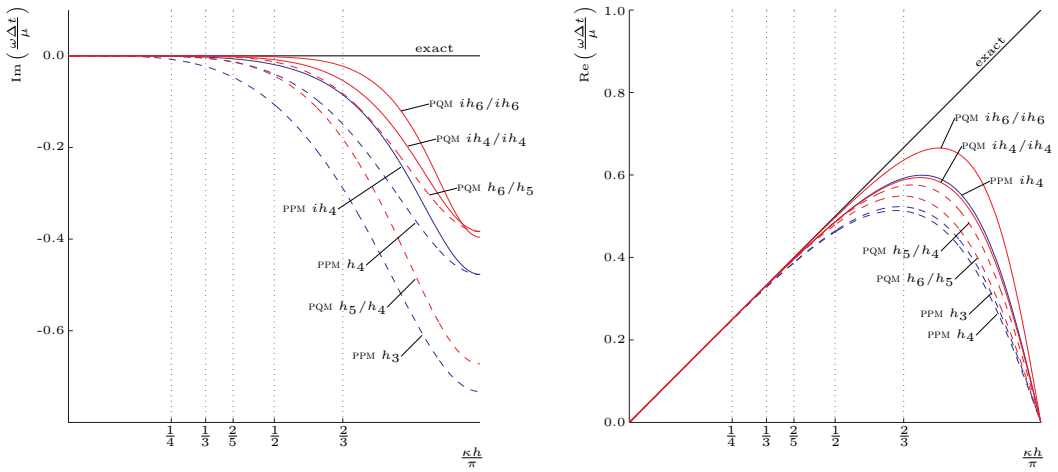

Figure 11: Dispersion relations for unlimited PPM and PQM advection schemes using Eq. (36), on uniform grids with a CFL number of 0.25. The left panel is indicative of numerical diffusion while the right panel shows the phase error. All explicit schemes are the most diffusive and feature the largest phase error for higher wavenumbers (shorter wavelengths) relative to the grid size. The best candidates are PPM ih_4 and PQM $ih6/ih6$, which introduce less numerical diffusion and exhibit better phase properties. PQM $ih4/ih4$ also has good properties but is only fourth-order accurate. To be noted is the underperforming phasal behavior of PPM h_4, which is the original PPM scheme. Schemes using explicit and implicit estimates for the edge values and slopes are represented with dashed and solid lines, respectively. Blue and red lines are used for PPM and PQM schemes, respectively. Shown values for $\frac{\kappa h}{\pi}$ are equivalent to wavelengths of, from left to right: $8h$, $6h$, $5h$, $4h$, $3h$ and $2h$.

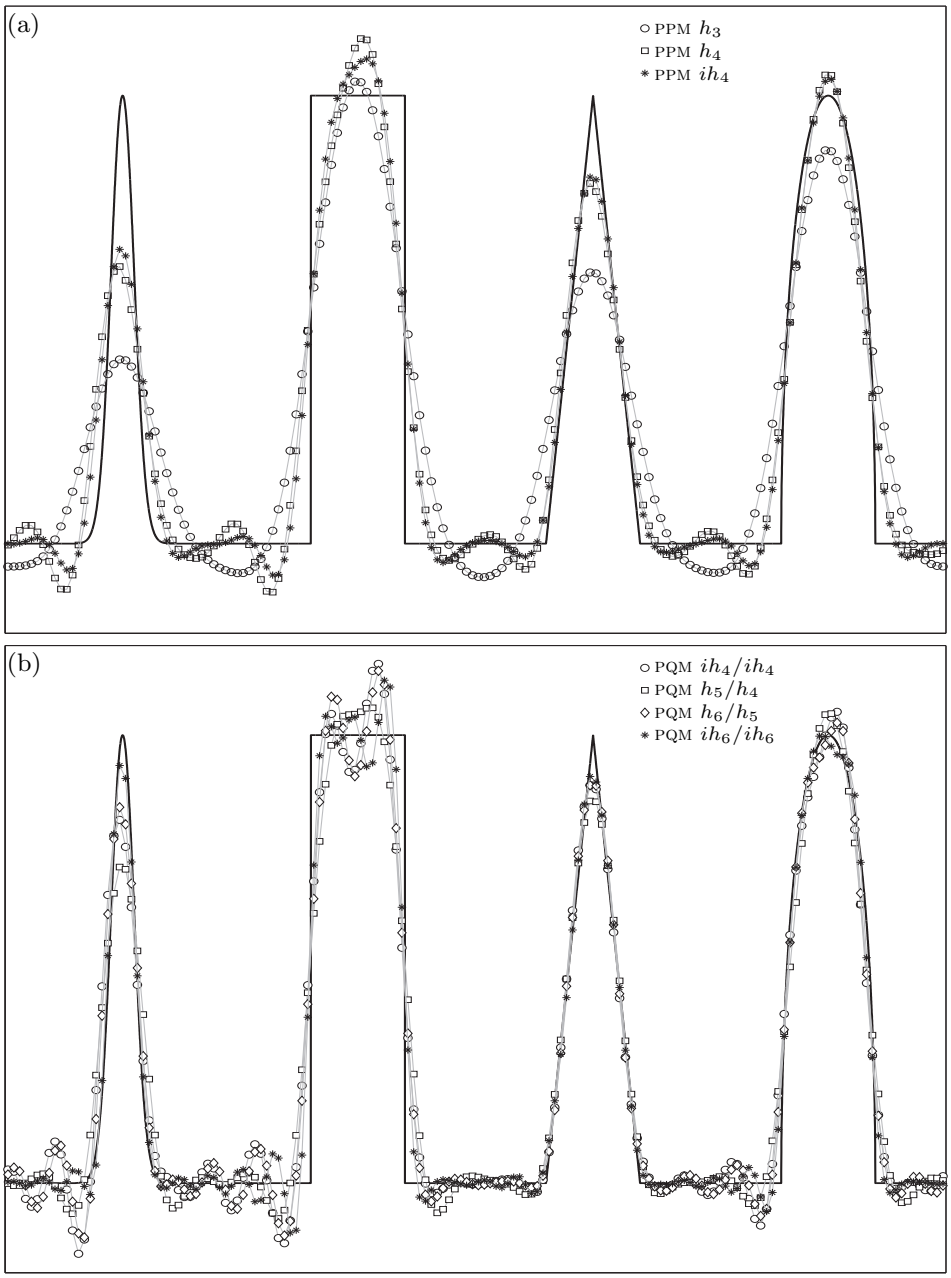

Figure 12: Unlimited advection experiments on uniform grids, in a periodic domain. Comparison of the advected solutions with the exact solution (black line) after 10 revolutions for a selection of unlimited (a) PPM schemes and (b) PQM schemes. The initial condition is given by Eq. 38. The grid has 160 cells and the CFL number is 0.25. The interpolation between cell averages is not the reconstructed profile and is drawn for visual convenience.

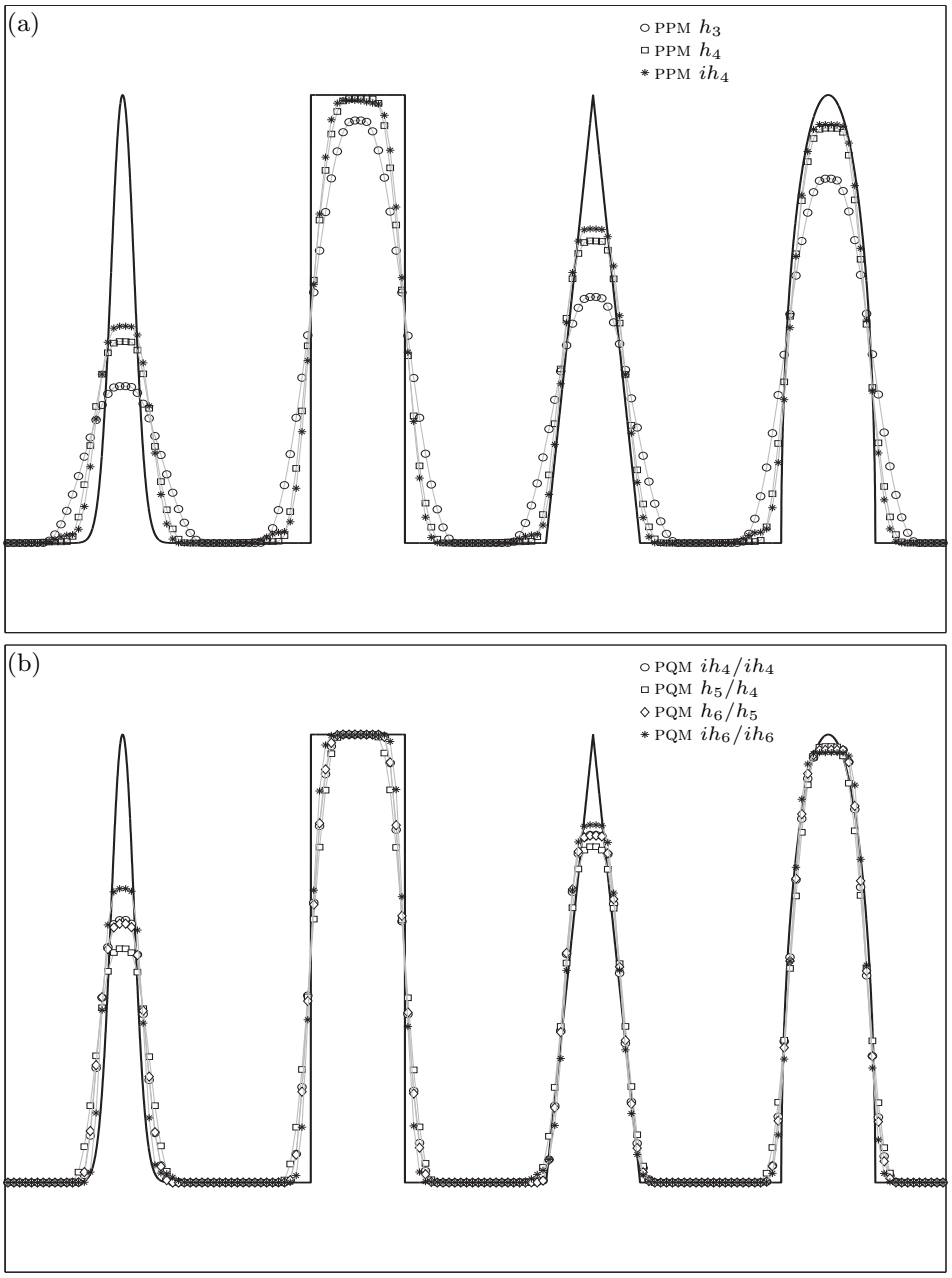

Figure 13: Limited advection experiments on uniform grids, in a periodic domain. Comparison of the advected solutions with the exact solution (black line) after 10 revolutions for a selection of limited (a) PPM schemes and (b) PQM schemes. The initial condition is given by Eq. 38. The grid has 160 cells and the CFL number is 0.25. The interpolation between cell averages is not the reconstructed profile and is drawn for visual convenience.

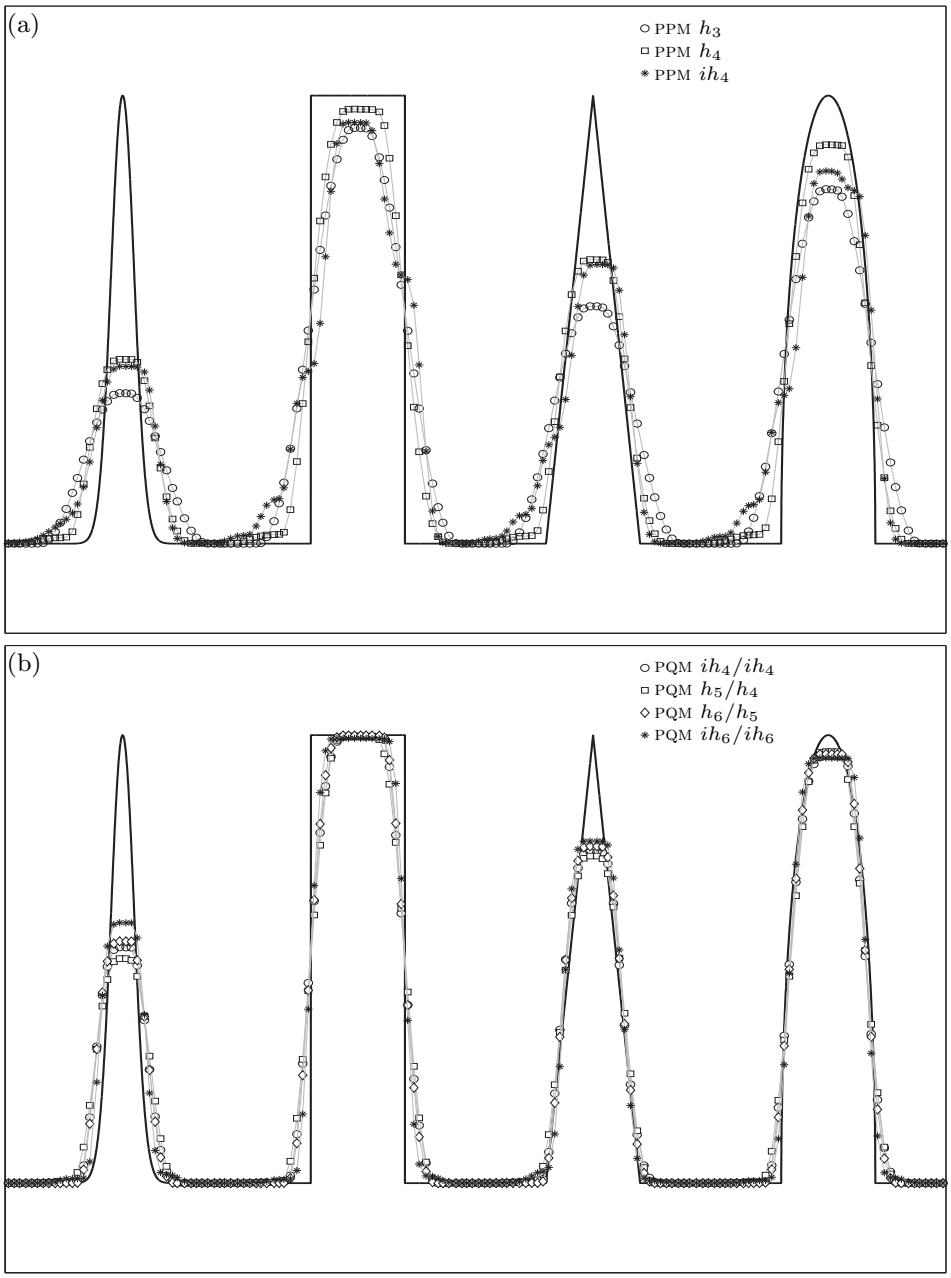

Figure 14: Limited advection experiments on nonuniform grids, in a periodic domain. Comparison of the advected solutions with the exact solution (black line) after 10 revolutions for a selection of limited (a) PPM schemes and (b) PQM schemes. The initial condition is given by Eq. 38. The grid has 160 cells and the CFL number is 0.25 relative to the smallest grid cell. The interpolation between cell averages is not the reconstructed profile and is drawn for visual convenience.

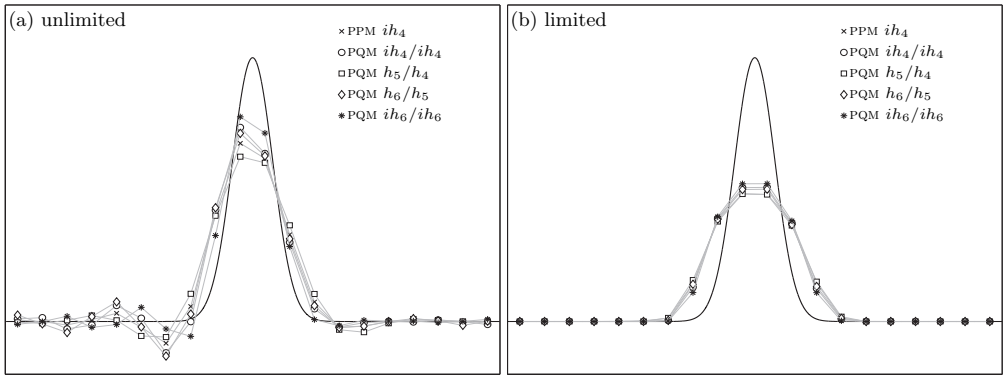

Figure 15: Advection of a Gaussian on a low-resolution uniform grid containing 20 cells. The domain is periodic and results are shown after one revolution (CFL number is 0.25). (a) The unlimited PPM ih_4 scheme outperforms PQM h_5/h_4, the latter being slightly more diffusive as suggested by the dispersion analysis in Figure 11. (b) The limitation of PPM ih_4 somewhat inhibits its intrinsic performance, as it now performs similarly to PQM h_5/h_4. The interpolation between cell averages is not the reconstructed profile and is drawn for visual convenience.

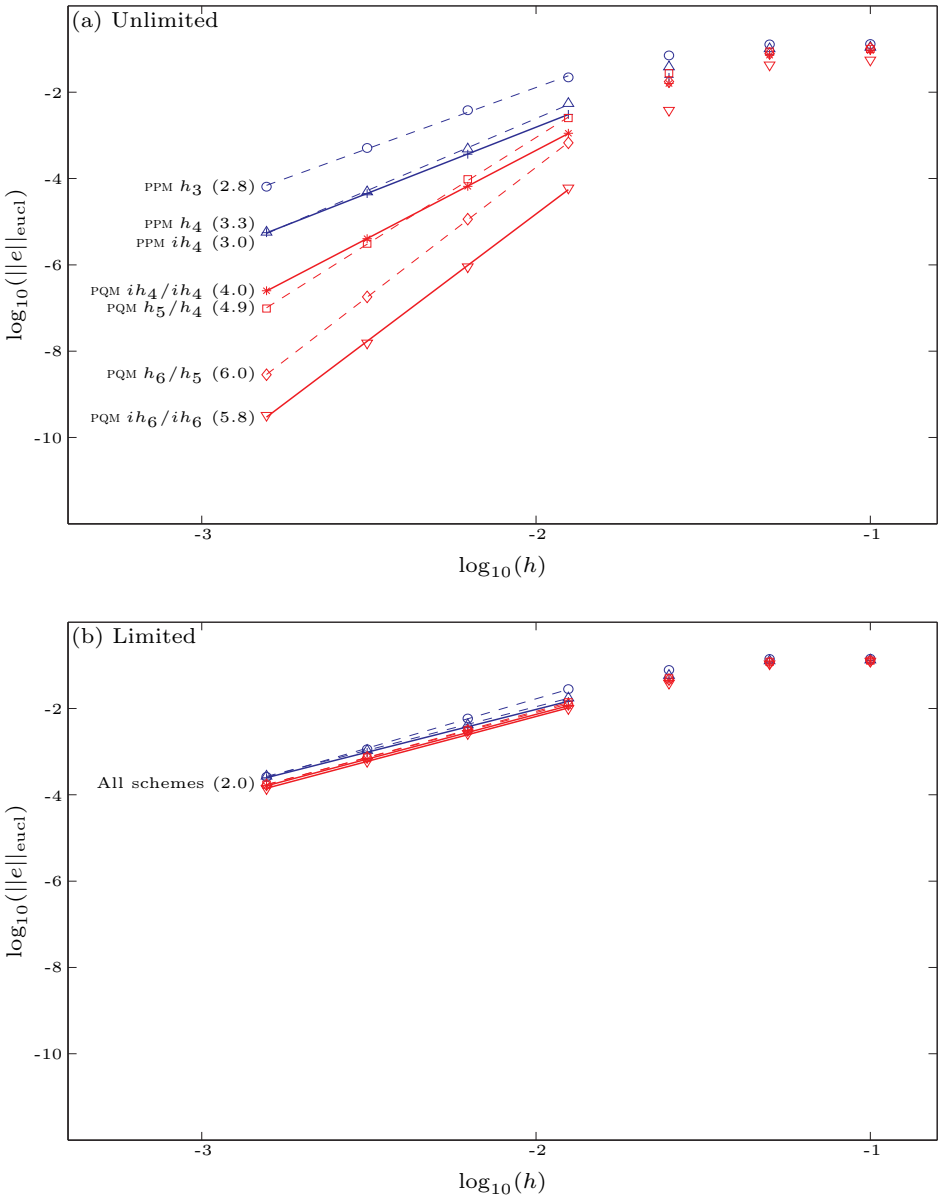

Figure 16: Orders of accuracy of (a) unlimited and (b) limited advection schemes for a Gaussian on uniform grids. Convergence rates are given next to the scheme name, between parentheses, and are established with respect to the Euclidian norm defined by Eq. (39). The convergence rates are roughly the same on nonuniform grids and are not shown. Note the sixth-order accuracy of PQM h_6/h_5 and PQM ih_6/ih_6. Also, notice how PQM ih_4/ih_4 performs better than PQM h_5/h_4 at lower resolution but is outpaced at higher resolution. The convergence rates for the unlimited schemes are the same as that obtained for unlimited reconstruction in Figure 5. The resolution of the Gaussian extremum is only second-order accurate, which is dominant for limited schemes.

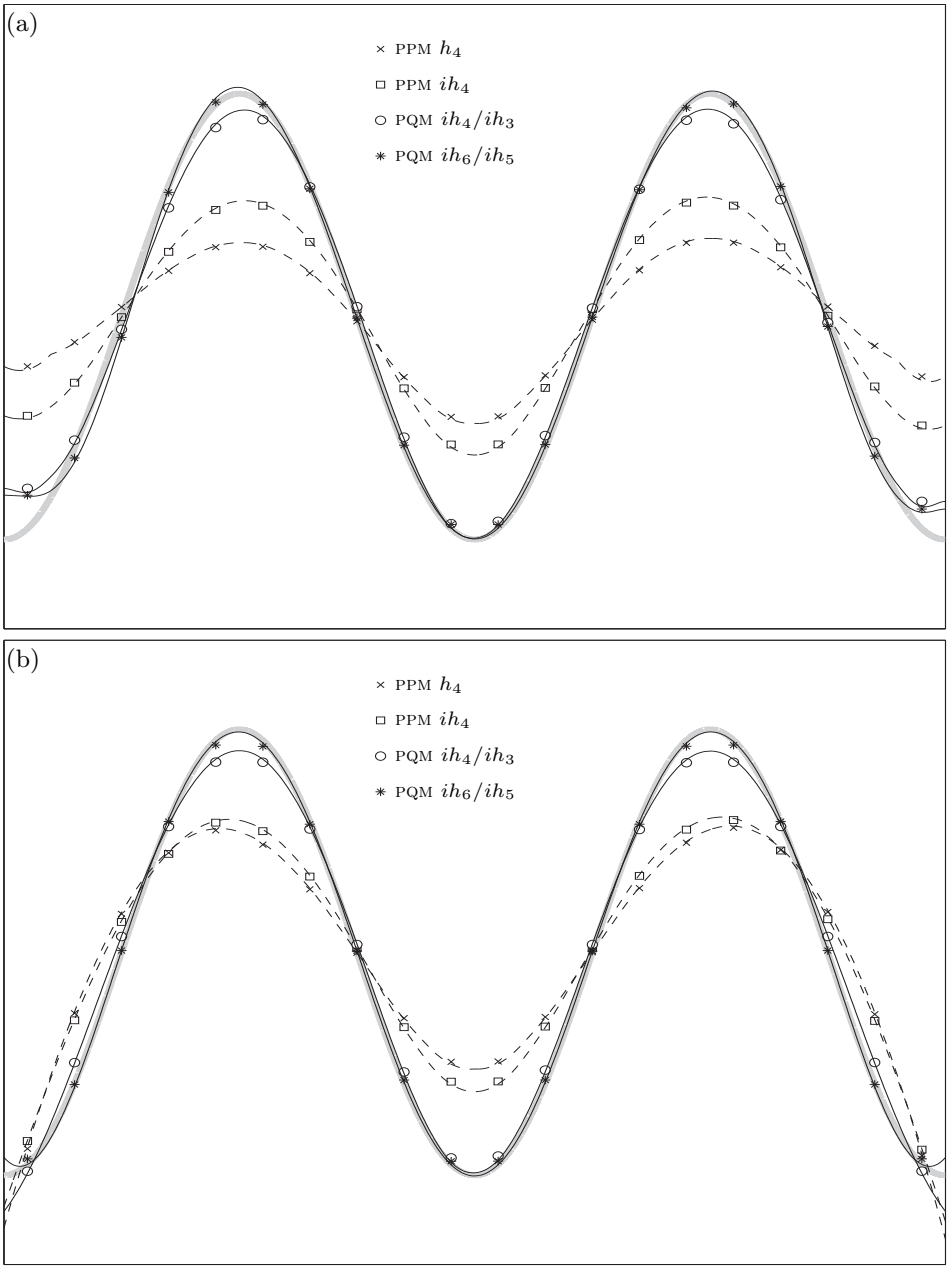

Figure 17: Unlimited remapping experiments in a closed domain using (a) low-order boundary conditions and (b) high-order boundary conditions. Each remapping cycle comprises the following steps: (i) reconstruction on a uniform grid composed of 20 cells, (ii) remapping onto a nonuniform grid composed of 18 cells that changes at each cycle, (iii) reconstruction on the nonuniform grid and (iv) remapping back onto the uniform grid. The light gray, thick line is the exact solution and the black thin lines represent the reconstructed profiles on the uniform grid, shown after 1000 remapping cycles. Notice the strong influence of the boundary conditions on the overall results.

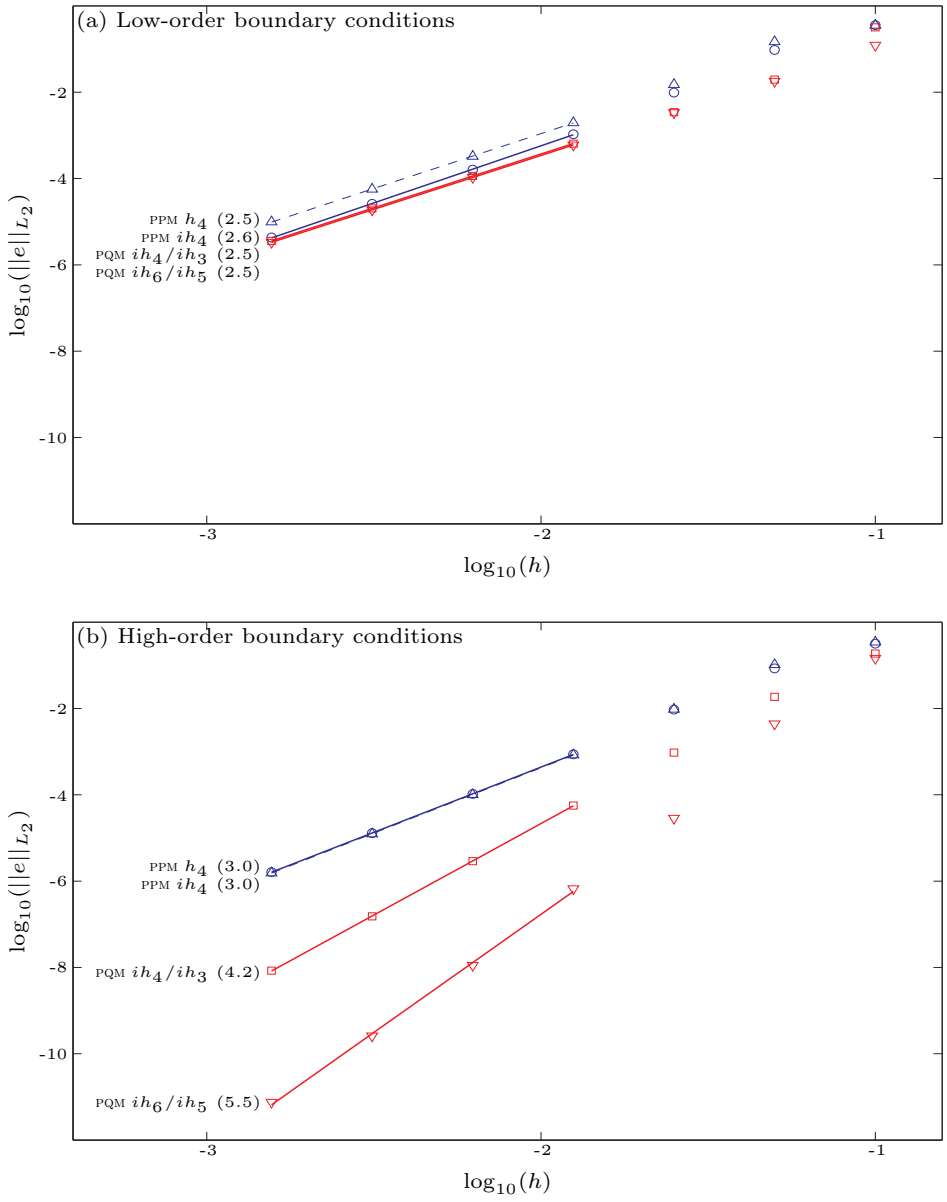

Figure 18: Convergence analysis for the unlimited experiment described in Figure 17 and carried out on gradually finer grids. For each grid, 500 remapping cycles are conducted and the L_2-norm of the error is computed between the exact and reconstructed profiles. (a) Low-order boundary conditions are used, which reduces the convergence rate down to 2.5 for all schemes. (b) High-order boundary conditions allow to preserve the nominal order of accuracy of all schemes.